63-4-1
Copy No. 13 of

ARF 407 304

ARMOUR RESEARCH FOUNDATION OF ILLINOIS INSTITUTE OF TECHNOLOGY
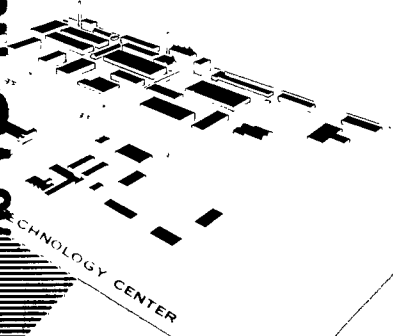
DDC

JUN 22 1963

TISIA B

NOTE: Effective June 1, 1963,
the name of Armour Research
Foundation of Illinois Institute
of Technology will change to
IIT RESEARCH INSTITUTE.

EVALUATION AND IMPROVEMENT OF RADAR

BEACON SYSTEMS

Report No. 3
Contract No. DA 36-039 SC-90693
DA Project No. 3C16-19-001
ARF Project No. E179
Third Quarterly Progress Report
1 December 1962 - 28 February 1963

U. S. Army Electronic Res. and Dev. Lab.
Fort Monmouth, New Jersey

EVALUATION AND IMPROVEMENT OF RADAR

BEACON SYSTEMS

Report Nr. 3

Contract No. Da 36-039 SC-90693
ARF Project No. E179

SMSA-RD-EID-013, 19 January 1962

DA Project No. 3C16-19-001

Third Quarterly Progress Report
1 December 1962 - 28 February 1963

The object of this study program is to establish
system parameters and technical specifications
for a coherent beacon and to determine the feasi-
bility of using tunnel diodes, varactor diodes, and
other solid state devices to advance the art of
radar beaconry.

Prepared by

J. Feldman
S. Kazel
R. Standley
P. Toulios

of

ARMOUR RESEARCH FOUNDATION
of Illinois Insitute of Technology
Technology Center
Chicago 16, Illinois

for

U. S. Army Electronics Res. and Dev. Lab.
Fort Monmouth, New Jersey

TABLE OF CONTENTS

TABLE OF CONTENTS (cont'd)

LIST OF ILLUSTRATIONS

EVALUATION AND IMPROVEMENT OF
RADAR BEACON SYSTEMS

PURPOSE

The program is concerned with two diverse areas relating to radar-beacon systems: 1)   solid state microwave component design and evaluation and 2)   coherent radar beacon system analysis.   Included as a part of the first area is the establishment of design criteria for those solid state devices which could be used advantageously in radar-beacon systems.   The analysis of the coherent beacon has been undertaken to permit quantitative evaluation of achievable system performance and to establish a basis for performance specification for future equipment developments.

EVALUATION AND IMPROVEMENT OF
RADAR BEACON SYSTEMS

ABSTRACT

Theory and experimental results of a varactor tuned C-Band Tunnel Diode Oscillator are presented. Work on C-band amplifiers is discussed with experimental results.

The dc biasing circuit of a c-band tunnel diode amplifier is analyzed and experimental results are obtained. The effect of instability in the biasing circuit is also discussed.

The fundamental limitations on the range and accuracy of coherent pulsed radar-beacon systems are analyzed. Specifications and design objectives for a coherent beacon are presented.

FACTUAL DATA

EVALUATION AND IMPROVEMENT OF

RADAR BEACON SYSTEMS

I. INTRODUCTION

This program is divided into two phases. One phase, covered in Section A, is concerned with fundamental limitations of coherent radar-beacon systems and coherent beacon parameter specifications. The second phase, covered in Section B, is concerned with improved components for radar beacons.

II. TECHNICAL DISCUSSION

A. Coherent Radar-Beacon System

1. General

This phase of the program is concerned with establishing the fundamental advantages and limitations of coherent radar-beacon tracking and with specifying the parameters required of a coherent beacon. In the previous Quarterly Reports the following fundamental limitations of coherent radar tracking were analyzed:

1. Velocity errors due to unavoidable instabilities in radar transmitter frequency. The rms velocity error is given by:

$$(\Delta v)_{ms} = \begin{cases} \dfrac{1}{\sqrt{2}} \dfrac{c}{\omega T} \sqrt{\tau/T}_c \;, & \tau < T \\[3mm] \dfrac{1}{\sqrt{2}} \dfrac{c}{\omega T} \sqrt{T/T}_c \;, & \tau > T \end{cases} \tag{1}$$

where c = velocity of light ($\sim 10^9$ ft/sec), ω = r-f frequency (radians/sec), T = smoothing time, τ = two-way propagation delay, and

T_c = period of coherence of radar transmitter (time required for rms phase error to equal one radian).

2. Spectrum broadening of the Doppler signal due to radar transmitter frequency instability. The Doppler signal was shown to contain both a discrete spectral line and a continuous, spread, spectrum.

The fractional power in each component was shown to be

$$P \text{ (discrete)} = \frac{1}{2} e^{- \tau/T_c} \tag{2}$$

$$P \text{ (continuous)} = \frac{1}{2} \left(1 - e^{-\tau/T_c}\right) \tag{3}$$

The continuous spectrum $v_n^2 (\omega_n)$ has the following form:

$$v_n^2 (\omega_n) = \frac{1}{1 + \omega_n^2} \left\{ 1 - e^{-r} \left[\cos (r\,\omega_n) + r\, \frac{\sin (r\,\omega_n)}{(r\,\omega_n)} \right] \right\} \tag{4}$$

where $\omega_n = (\omega - \omega_d)\, T_c$ is normalized frequency from band center, ω_d, and $r = \tau/T_c$ is normalized propagation delay.

3. Velocity errors due to frequency instability in the voltage-controlled oscillator (VCO) of the radar Doppler tracking loop. The errors decrease as the bandwidth of the Doppler tracking loop increases (opposite to the effect on receiver noise). The counter which "measures" the Doppler loop frequency output (i. e., averages Doppler frequency over successive time intervals of length T) must be included in the analysis, since, in its absence, the velocity error integral will not converge to a finite number.

We shall now consider several additional facets of coherent radar-beacon systems.

2. Coherent Pulse-Radar Tracking Modifications and Characteristics

a. Non-Coherent Range Tracking, Coherent-Velocity Tracking

A standard non-coherent range tracking system is shown in Figure 1 (enclosed in dashed line). The i-f pulses are envelope detected (i. e., non-coherently) and the range gate is forced to follow the incoming pulses by the feedback action of the so called "split gate" (or "N-squared" gate) range tracking loop (shown in detail in Figure 2(a)). The range gate is used to gate the i-f pulses, eliminating noise except for the duration of the pulse. Non-coherent velocity data may be obtained by differentiating range data (i. e., differentiating
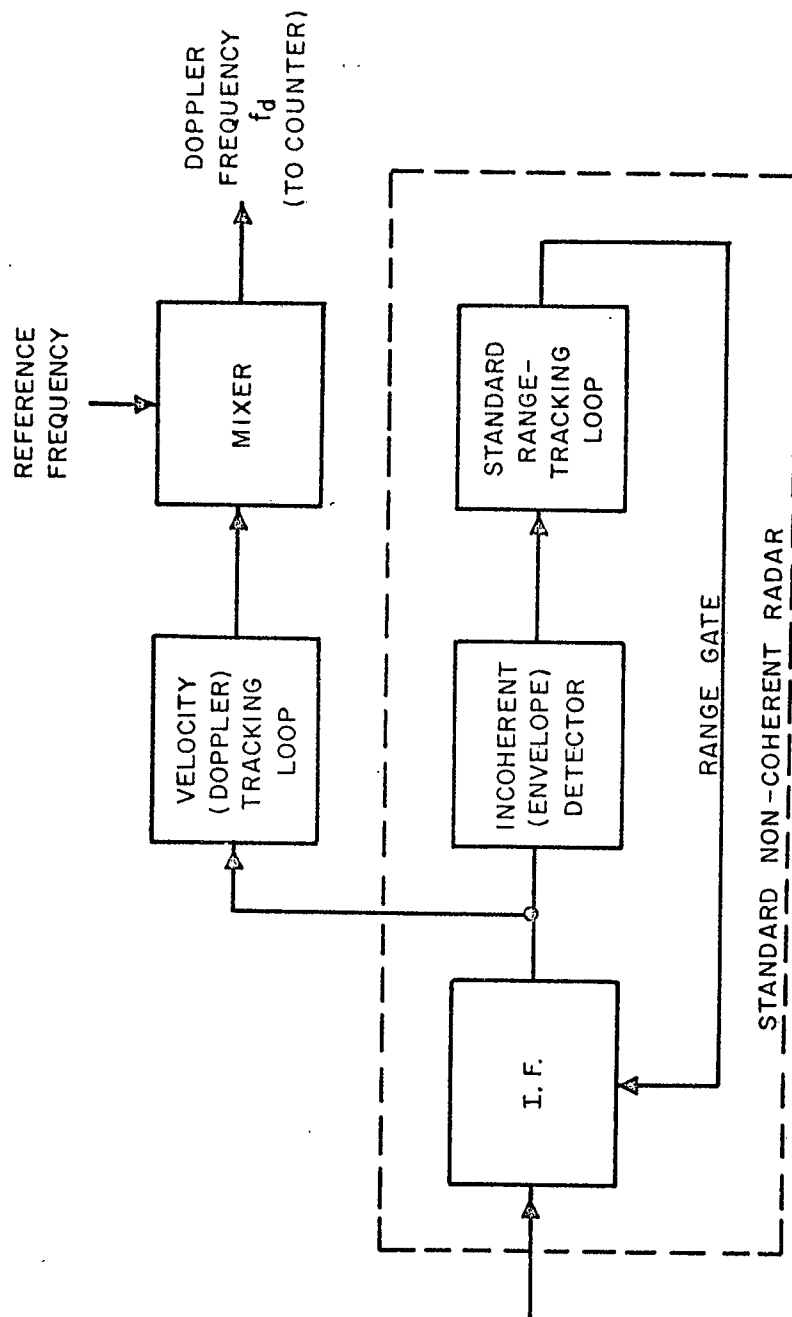
FIG. 1   NON-COHERENT RANGE TRACKING, COHERENT VELOCITY TRACKING

4

range gate position). Range gating is of importance, not only because the position of the range gate represents target distance, but because it reduces the output noise power in the range (and angle) tracking loops by the gating factor (i. e. , duty ratio).

Doppler (velocity) tracking is accomplished directly by frequency tracking of the gated i-f pulses in a Doppler tracking loop as indicated in Figure 1. . (Figure 2(b) shows the details of the coherent Doppler tracking loop.) Mixing with a reference frequency, as shown, is generally necessary to obtain the Doppler frequency signal, which may then be "measured" (by a counter, for example).

It is important to note that in the above system the Doppler channel has no effect on the operation of the (non-coherent) range tracking channel; the converse is not true since range gating of the i-f ulses into the Doppler channel is essential to provide a useable S/N ratio. Thus, the signal would first be acquired non-coherently in range and then would be acquired by the Doppler channel. In this system, the maximum tracking and acquisition range of the Doppler channel is limited to that of the non-coherent range tracking channel. This maximum range limitation normally occurs at a peak i-f S/N ratio somewhat above 0 db, since for lower values of S/N, the incoherent second detector rapidly degrades the S/N ratio.

b. Improvement in Tracking Accuracy Due to Coherency

Based upon the analysis of Doppler tracking performed previously[1], it can be shown (see Appendix A) that, at high input S/N ratios, the effective improvement in the voltage S/N ratio due to coherency, denoted by R, is

$$R = (\frac{1}{\sqrt{2}} f_o \tau) \tag{5}$$
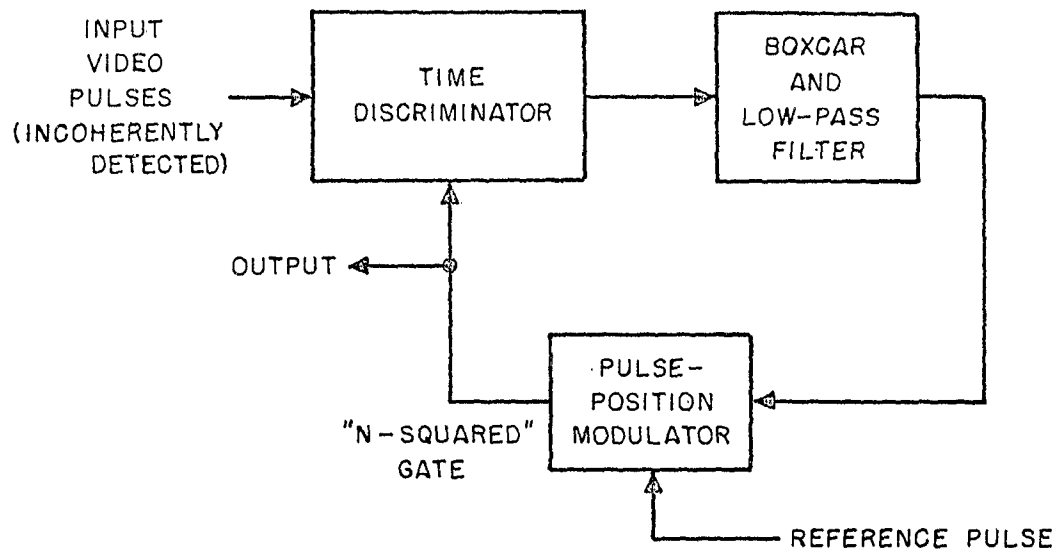
(a) RANGE TRACKING LOOP
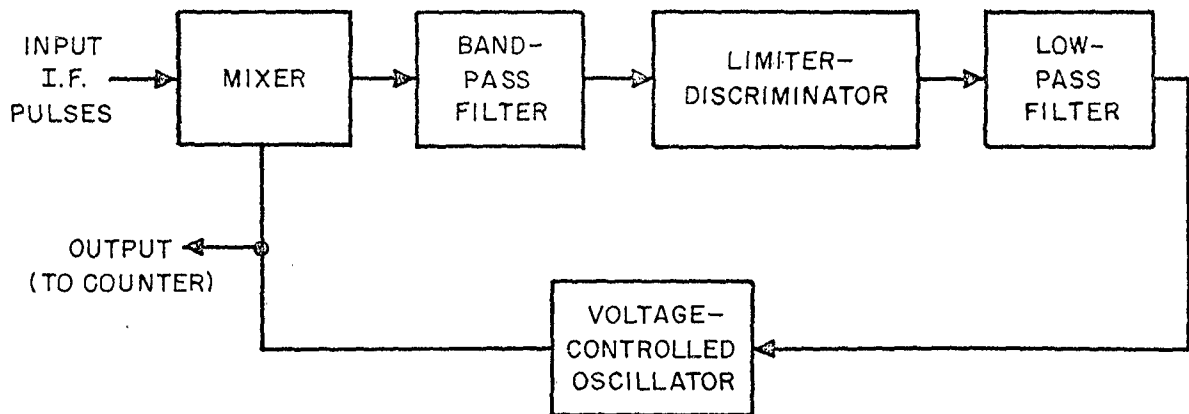
(b) VELOCITY (DOPPLER) TRACKING LOOP

FIG. 2   RANGE AND VELOCITY TRACKING LOOPS

where f_o is the transmitted frequency and τ is the pulse width. R-f frequency, f_o, appears in (5) because increasing f_o increases the Doppler shift, which corresponds to "signal" in the frequency tracking loop, without any increase in frequency jitter due to system noise. Pulse-width, τ, appears in (5) because all other things remaining equal, the tracking accuracy of a non-coherent radar decreases with increasing pulse width; the coeherent radar, whose inherent accuracy is unaffected by pulse width, therefore, becomes relatively more accurate than the non-coherent radar as τ increases.

For f_o = 5.65 kmc and τ = 0.25 microseconds, the effective improvement in S/N ratio is

$$R = (\frac{1}{\sqrt{2}} \, 5.65 \cdot 10^9 \cdot 0.25 \cdot 10^{-6}) = 1000 \ (60db). \tag{6}$$

As shown in Appendix B, the r.m.s. accuracy of velocity data of non-coherent pulse radar (obtained by differentiating range data) is approximately given by

$$\sigma_v = \frac{c \, \tau}{\sqrt{T^3 f_r} \cdot (V_s/V_n)} \tag{7}$$

where c = velocity of light, τ = pulse width, T = tracking loop smoothing time, f_r = PRF, and V_s/V_n = voltage S/N ratio. For τ = 0.25 microseconds, T = 0.1 second, f_r = 400, and V_s/V_n = 10 (20 db), the velocity accuracy of the non-coherent pulse radar is

$$\sigma_v = \frac{250}{\sqrt{0.4} \times 10} = 39.5 \ ft/sec. \tag{8}$$

A straight forward, but incorrect, application of the improvement factor of 1000 in Equation (6), would give a pulse-Doppler velocity accuracy of

$\sigma_v = 0.0395$ ft/sec.

The incorrectness lies in the fact that the improvement factor, R, of (5), and the velocity accuracy, σ_v , of (7), takes into account only the errors due to system noise. There are, in addition, velocity errors due to target lag (or lead), which are not included in (5) or (7). To achieve minimum tracking error, a non-coherent pulse radar will operate with a bandwidth for which lag errors and noise errors are comparable in magnitude. Coherent operation will reduce the noise errors by the large factor indicated in (5) and (6), but has no direct effect on the lag errors. To reduce the lag errors, the tracking bandwidth must be increased, until a condition is again reached in which noise and lag errors are comparable. In this re-optimization process, the increase in bandwidth prevents the noise from being reduced to the extent indicated by (5).

In the previous analysis of Doppler tracking[1], it was shown that to correctly derive the improvement factor of pulse-Doppler, the type of target motion must be specified. For a target motion consisting of random steps of velocity, the rms error, σ_v , in target velocity was found to be[1]

Non-coherent
radar
$$\sigma_v^8 = \frac{8}{16} c^2 V_{rms}^6 K^3 \tau^2 \eta / P_{av} \tag{9}$$

Coherent:
radar
$$\sigma_v^8 = \frac{16}{3} c^2 V_{rms}^6 K^3 \eta / P_{av} f_o^2 \tag{10}$$

where c = velocity of light, V_{rms} = rms target velocity, $K = 2/\overline{T}$, where $\overline{T}$ = average interval between velocity steps, τ = pulse width, η = input noise density, f_o = transmitted r-f frequency, and P_{av} = average power of

received echo. The improvement factor, F, the ratio of non-coherent to coherent velocity errors, is found from (9) and (10) to be

$$F = \left(\frac{1}{\sqrt{2} \, f_o \mathcal{T}} \right)^{1/4} \tag{11}$$

Instead of a factor of 1000, the improvement is only 5.62.

For random steps of acceleration, the rms error in target velocity was found to be

Non-coherent: $\quad \sigma_v^4 = \frac{3}{2} \, c^2 \, A_{rms}^2 \, K \eta \mathcal{T}^2 / P_{av}$ (12)
radar

Coherent: $\quad \sigma_v^4 = 3 \, c^2 \, A_{rms}^2 \, K \eta / P_{av} \, f_o^2$ (13)
radar

The improvement factor in this case is

$$F = \left(\frac{1}{\sqrt{2}} \, f_o \mathcal{T} \right)^{1/2} \tag{14}$$

For the same values of f_o and $\mathcal{T}$ used previously, F = 31.6.

Thus, in general, the improvement factor obtainable appears to be less than the factor $\left(\frac{1}{\sqrt{2}} \, f_o \, \mathcal{T} \right)$. It should be noted that although increasing the pulse width, $\mathcal{T}$, increases the improvement factor, F, it does not, in itself, increase the accuracy of the coherent radar, since (10) and (13) are independent of $\mathcal{T}$; increasing $\mathcal{T}$ only degrades the accuracy of the non-coherent radar and the coherent radar is only improved by comparison.

As a sample calculation, consider the velocity error of (8) caused by noise in a non-coherent radar. Assume that an equal error results from lag, giving a total error of $39\sqrt{2}$ = 56 ft/sec. If the target motion consists of random steps of acceleration, then the improvement factor (for the previously assumed values of f_o and $\mathcal{T}$) is 31.6 and the rms velocity error of the coherent system

is   56/31.6 = 1.8 ft/sec.

c. Comparison of Threshold of Range and Velocity Tracking

Non-coherent range tracking will normally have a threshold somewhat above 0 db i-f S/N ratio (peak signal to rms noise). The reason is that the non-coherent second detector, which converts i-f to video, rapidly degrades the S/N ratio when the input falls below 0 db. Similarly, the frequency discriminator of the velocity tracking loop will also rapidly degrade the S/N ratio when the input S/N ratio to the discriminator falls below 0 db. It would therefore appear that range and velocity tracking would have approximately the same threshold. This is not the case, however, because an improvement in S/N ratio takes place when the pulsed signal in the i-f is converted into a c-w signal by the bandpass filter of the velocity tracking loop. As shown in Appendix C , the improvement factor (for voltages S/N ratio) is given by

$$\sqrt{f_r/B_{bp}} \tag{15}$$

where f_r is PRF and B_{bp} is the width of the bandpass filter. Since the ratio f_r/B_{bp} is commonly considerably greater than unity, an improvement in S/N ratio occurs. Thus, the non-coherent range tracking loop would appear to limit the maximum range of the coherent radar, although within this range the coherent velocity tracking loop will provide increased accuracy in velocity data. A method for partially overcoming the maximum range limitation of the non-coherent range tracking loop is discussed in the following section.
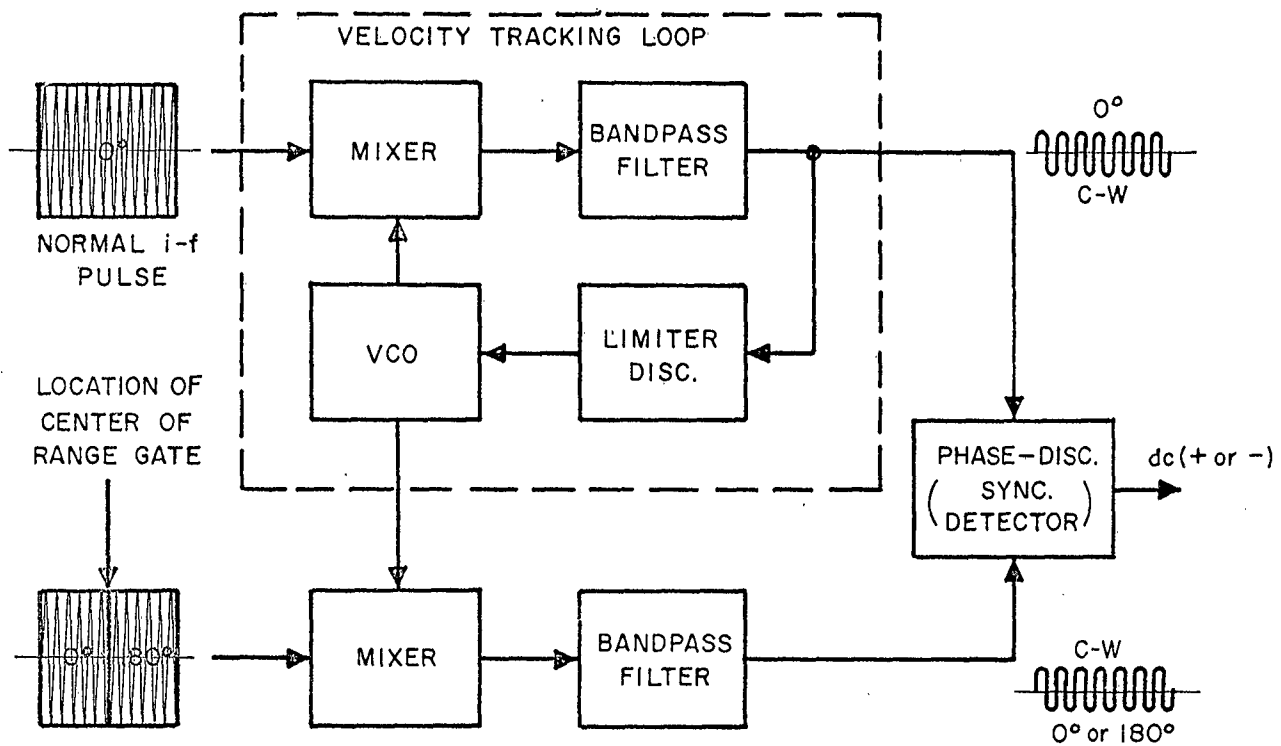
d. Fine-Line Range Tracking

The normal acquisition procedure for a coherent, pulse-Doppler radar would be to first acquire (lock-onto) the target range, using the standard, non-coherent range tracking loop. After acquisition in range, the echo pulses would be gated into the Doppler tracking loop and acquired (locked onto) in

ARMOUR RESEARCH FOUNDATION OF ILLINOIS INSTITUTE OF TECHNOLOGY

velocity. Once velocity acquisition has taken place, it is possible to use the Doppler information to improve the S/N ratio of the range tracking loop to the higher level existing in the velocity tracking loop. This procedure has been referred to as "fine-line" range tracking.[2]

The technique of fine-line range tracking is shown in Figure 3a. It is assumed that acquisition of the Doppler signal has taken place in both the range tracking loop and the velocity tracking loop (the dashed box). In a parallel channel, the normal i-f pulse is reversed in phase at the instant corresponding to the center of the range gate. The "split-phase" pulse is then mixed to the same frequency and subjected to the same filtering as the input to the velocity tracking loop. The outputs of the band pass filters of the velocity tracking loop and of the "split-phase" channel are coherent, c-w signals. The two c-w signals will be either in phase or 180 degrees out of phase depending on whether the phase reversal takes place after or before the center of the i-f pulse. If the phase transition occurs exactly at the center of the i-f pulse, the c-w contributions of the early and late halves of the split pulse will cancel, resulting in zero amplitude c-w signal and zero voltage out of the phase discriminator. As the point of phase transition occurs further from the center, the amplitude of the net c-w signal will build up in direct proportion, with a fixed phase of 180 degrees for early transitions and a fixed phase of 0 for late transistions. Thus, the phase discriminator will produce the linear, bi-polar characteristic desired of a range discriminator, as indicated in Figure 3b.

An improvement in S/N ratio and a consequent lowering of the threshold takes place in the fine-line range tracking system described above. The reason for this is that, as discussed previously, conversion of the pulsed

(a) BLOCK DIAGRAM
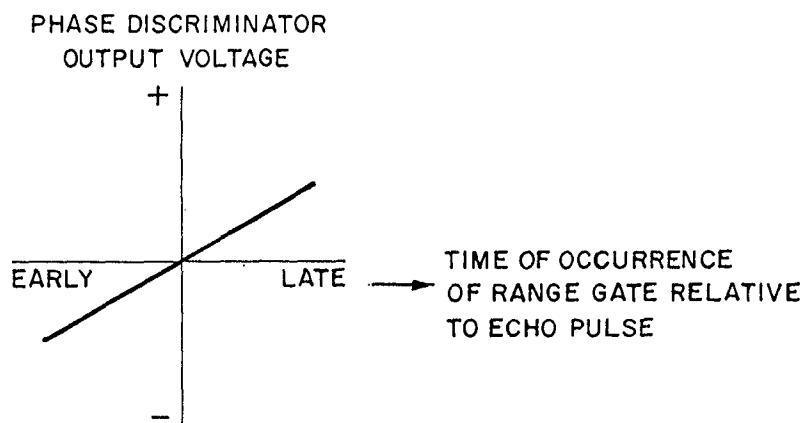
(b) RESULTANT RANGE DISCRIMINATOR CHARACTERISTIC

FIG. 3   FINE-LINE RANGE TRACKING

echo signal into c-w improves the voltage S/N ratio by the factor

$$\sqrt{f_r / B_{bp}}.$$

Both inputs to the phase discriminator have been converted to c-w by the
action of identical narrow band-pass filtering and therefore are both improved
to the above extent.

The action of the fine-line range tracking system has sometimes been
referred to as "coherent" range tracking, implying that the phase-discriminator
acts as a coherent (or synchronous) detector. Ordinarily, coherent detection
implies that one input to the phase-discriminator the "reference" is noiseless,
or much less noisy, then the other input, the "signal". This is not the case
for the fine-line range tracker where both inputs to the phase discriminator,
although improved in S/N ratio by narrow band filtering, are equally noisy.
Also, since essentially the same noise is present in both inputs, the
multiplication effected by the phase discriminator comes close to being
equivalent to square-law, or incoherent detection. When the two noisy c-w
input to the phase discriminator fall to about 0 db S/N ratio, a threshold
effect will set in, which would not occur if true coherent detection were involved.
Thus, the improvement in performance due to fine-line tracking should be
attributed to the increased S/N ratio resulting from narrow band filtering,
and not to the use of the phase discriminator.

The same performance could be obtained without a phase dicriminator
as follows. Let the position of the range gate divide the i-f pulse into an early
and a late portion. Gate each portion into a separate velocity tracking loop
and rectify and subtract the output of the narrow band filters in each loop.
When the range gate is centered on the i-f pulse, the outputs of the two channels

will be equal, giving a zero difference signal. For other positions of the range gate, the difference will be either increasingly positive or negative, giving a linear range discriminator characteristic, the same as that shown in Figure 3b. Since narrow band filtering occurs in each loop, the same S/N improvement will occur as in the previously described fine-line tracking technique, and the performance of the two systems will be equivalent. The use of two tracking loops is more complex and would require equalization of the gain of the two channels; thus, as a practical matter, it is a less desirable approach. However, it does demonstrate that the narrow band filtering, and not the use of a phase discriminator, is the basis of the improved S/N ratio of fine-line range tracking.

With fine-line range tracking, the S/N ratio is improved to essentially the same value as in velocity tracking, so that range tracking can be maintained out to a greater range than is possible with non-coherent range tracking. The effective increase in voltage S/N ratio is the factor

$$\sqrt{f_r/B_{bp}}.$$

Unfortunately, if target track were lost at the extended range, the non-coherent range tracking loop would be unable to re-acquire the target because the input S/N ratio would be below its threshold. Re-acquisition of the target at extended range could be accomplished by a simultaneous search in range, velocity and angle, with lock on occuring first in the Doppler tracking loop. However, the time required to search in three variables, range, angle, and velocity will be greater than for non-coherent radar, where only range and angle are involved. Whether re-acquisition is practical will probably depend on whether, in a particular situation, the quantities range, angle, and velocity are known to a

sufficient approximation to permit a successful search.

Thus fine-line tracking cannot be said to provide an unqualified extension of radar range. If fine-line tracking is initiated at normal ranges, then tracking can be continued out to extended ranges. However, acquisition at extended range will be more time consuming and, possibly, impractical in some cases.

3. Coherent Beacon Parameters

a. General

The distinguishing feature of a coherent beacon is that its reply is phase coherent with the interrogation. That is, the reply and interrogation pulses have either no phase difference or at most a fixed phase difference. A coherent beacon thus acts essentially as an r-f amplifier.

A non-coherent beacon, on the other hand, detects the envelope of the interrogation pulse. The detected video pulse triggers a modulator; which initiates oscillations in the transmitting tube. Since the phase with which an oscillator starts up is ordinarily random (due to the effects of oscillator noise), the non-coherent beacon replies with random phase, even when interrogated by r-f pulses which are coherent from pulse-to-pulse.

Thus, it is seen that a coherent beacon is necessary if the phase of the interrogations from a coherent radar are to be preserved. Since Doppler frequency is the rate of change of phase, use of a coherent beacon permits Doppler frequency to be extracted. From the Doppler shift relation

$$f_d = 2 v/\lambda$$

the target velocity may be determined directly (rather than by differentiating range data).

A beacon cannot be designed in isolation. Its design can only proceed by considering it as part of the entire radar/beacon tracking system. The same could be said for the beacon tracking radar. However, in practice, the beacon is usually designed with a specific radar (or class of radars) in mind, rather than vice versa. In the present study it is desired to arrive at parameter specifications and design goals for a coherent beacon which will be compatible, primarily, with the proposed coherent modification of the AN/FPS-16 radar

ARMOUR RESEARCH FOUNDATION OF ILLINOIS INSTITUTE OF TECHNOLOGY

and with the coherent AN/FPQ-6 radar. Secondarily, it is desired that the coherent beacon for compatible with existing non-coherent radars such as the unmodified AN/FPS-16.
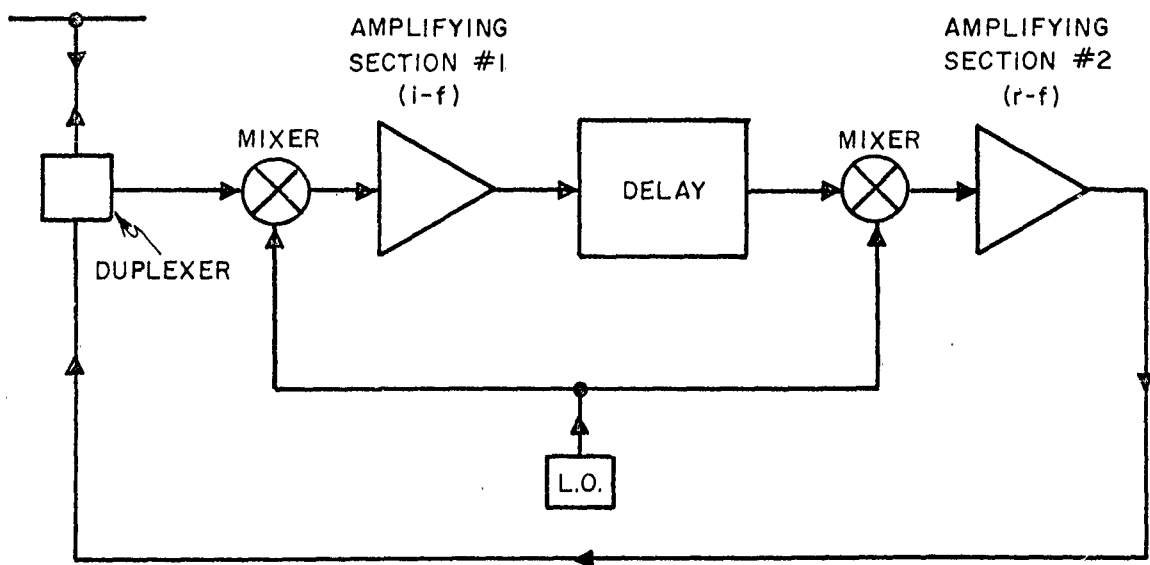
b. Operation of the Coherent Beacon

The basic elements of a coherent beacon are shown in Figure 4(b). It is instructive, however, to consider first the coherent "augmenter" of Figure 4(a). The agumenter consists of an r-f amplifier connected to the antenna by means of a duplexer. The maximum gain of the augmenter is limited by the isolation afforded of the duplexer. Greater gains would cause the system to oscillate at r-f. The relatively low gain of the augmenter limits its usefulness for beacon applications. However, advances in the state-of-the art of duplexing, making greater possible isolation, may ease this limitation.

The coherent beacon configuration of Figure 4(b) is intended to over-come the gain limitation of the augmenter. The basic approach is to divide the total amplification into two sections, keeping one or the other section off at all times so that the instantaneous loop gain is always zero, thereby removing feed-back and preventing oscillations. This mode of operation is possible because the pulsed signal is amplified sequentially, so that both amplifying sections need not be on at the same time.

The following is a more detailed description of the operation of the coherent beacon. The first, or input, amplifier is normally on, allowing it to receive the pulse and pass it, after mixing, into the delay line for "storage". The second, or output, amplifier is normally off. While the i-f pulse is in storage in the delay line, the input amplifier is turned off and the output amplifier is turned on. When the i-f pulse emerges from the delay line, it is mixed up to r-f and fed to the output amplifier, which is by then fully operational. The
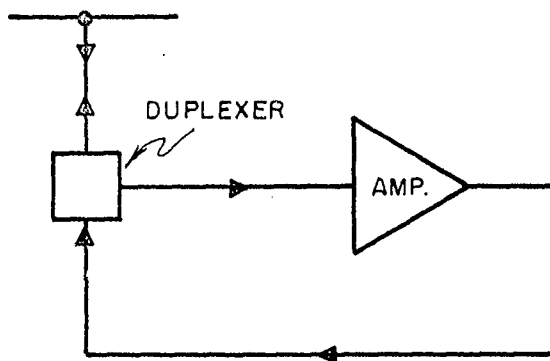
(a) AUGMENTER

(b) COHERENT BEACON

FIG. 4   COHERENT BEACON CONFIGURATION (SIMPLIFIED)

18

amplified r-f pulse is then applied to the antenna for transmission. After transmission of the pulse, the coherent beacon reverts to its normal condition with the output amplifier off and the input amplifier on, ready to receive the next pulse. A block diagram of the coherent beacon is given in Figure 5.

It should be observed that whereas an augmenter has no lower threshold, the coherent beacon described herein does. No beacon output is obtained unless the input signal is sufficiently strong to trigger the video circuits. which turn the input and output amplifiers on and off. The presence of this input threshold requires that the interrogation link be somewhat stronger than the reply link if the threshold is not to limit the range of the system. This condition will usually exist, since ground radar transmitters are typically high power, while beacon power output is low by comparison.

c. Parameter Specifications and Design Goals

As indicated previously, the parameter specifications of the coherent beacon will be greatly affected by the characteristics of the AN/FPS-16 and AN/FPQ-6 radars, which will be capable of utilizing the coherent nature of the beacon echo, and secondarily, by the characteristics of non-coherent radars, such as the unmodified AN/FPS-16, which may track the beacon without utilizing the coherency. The characteristics of these radars are given in Appendix D .

A set of parameter specifications and design goals for a coherent beacon is presented in Table I . Following this are the justifications for the parameters selected.

DUPLEXER TRIGGER

ANTENNA

DUPLEXER

MIXER

I.F. AMP.

VIDEO
DETECTOR
AND
AMPLIFIER

THRESHOLD

GATE
GEN.

LOCAL
OSC.

I.F.
DELAY

MIXER

I.F. AMP.

R.F.
AMP.

MODULATOR
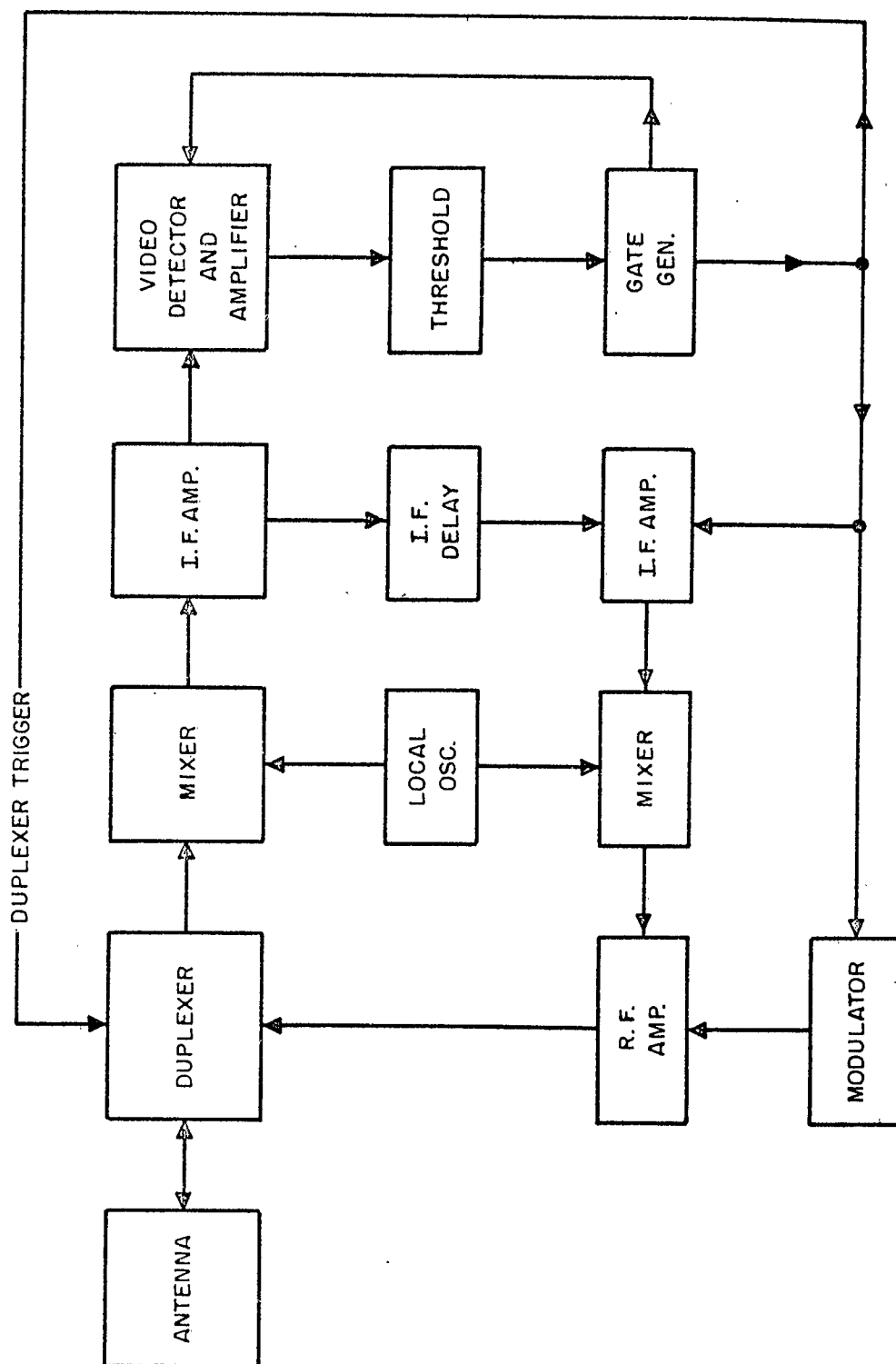
FIG. 5   BLOCK DIAGRAM OF COHERENT BEACON

20

TABLE I

PARAMETER SPECIFICATION AND DESIGN GOALS

FOR A COHERENT BEACON

Frequency Range	5400-5900 megacycles
Bandwidth	6.0 megacycles
Noise Firing Rate	10 per second
Sensitivity	-91 dbm
Duty Cycle	0.12
Delay	5.0 microseconds
Delay Variation	0.01 microseconds
Jitter	0.01 microseconds
Phase Stability	3.0 degrees
Frequency Stability	0.250 cps in 5 microseconds
Recovery Time	25.0 microseconds
Power Output	4.0 watts (for 250 mile range) 400 watts (for 2500 mile range) (based on use with AN/FPS-16 radar modified for 2.4 μs pulse)

d. Justification of Parameter Choices

1. Frequency Range: 5400-5900 megacycles

 To be compatible with the AN/FPQ-6 and AN/FPS-16 radars.

2. Bandwidth: 6.0 Mc

 For a pulse width, τ, the optimum (matched filter) i-f bandwidth for maximum S/N ratio is on the order of

$$B_{if} = 1/\tau$$

For the 2.4 μs width of the AN/FPQ-6 radar, $B_{if} = 0.4$ mc. However, in order to preserve a rise time of at least 0.25 μs, and to preserve some response for 0.25 μs pulse width, a bandwidth of 4.0 mc should be used (Fast rise time is necessary if limiting is not to introduce large variations in delay). Allowing 1.0 mc for Doppler and 1.0 Mc for drift and mistuning gives a total bandwidth of 6.0 Mc.

3. Noise Firing Rate: 10/sec

 This figure is not critical, since a large change in noise firing rate corresponds to only a small change in S/N ratio. However, it should be kept down to a small fraction of the maximum interrogation rate to prevent overloading of the beacon power output tube. Assuming a maximum of five interrogating radars with average PRF of 1000, for a total interrogation rate of 5000, the addition of 10 noise firings/sec should be acceptable.

4. Sensitivity: -91 dbm

 (See Appendix H)

ARMOUR RESEARCH FOUNDATION OF ILLINOIS INSTITUTE OF TECHNOLOGY

5. Duty Cycle: 0.12

Based on five simultaneoulsy interrogating radars, each with average PRF of 1000, and pulse width of 2.4 microseconds.

6. Delay: 5.0 microseconds

To allow sufficient time before reply to receive the widest pulse, 2.4 microseconds.

7. Delay Variation: 0.01 microseconds

Provided the coherent beacon is operated as a _linear_ amplifier, it has the potential to preserve a constant output pulse shape, independent of input level. Some form of Instantaneous Automatic Gain Control (IAGC) will be necessary if full beacon power output is also to be achieved over the entire range of inputs. The maximum delay variation of 0.01 microseconds is in the nature of a design goal; whether it can even be approached will depend on the feasibility of a suitable IAGC technique.

8. Jitter, Less than 0.01 microseconds

This specification refers only to jitter due to sources other than input noise. Jitter due to input noise is a natural and unavoidable phenomena and is determined by other considerations, primarily, the S/N ratio of the minimum triggering signal (which in turn is determined by such factors as minimum sensitivity, bandwidth, and false-alarm rate). Thus a separate specification on jitter due to input noise seems unnecessary.

9. **Phase Stability: Output phase must be within 3.0 degrees (rms) of input phase**

As shown in Appendix I , if coherent beacon local oscillator instability is to contribute less than 0.01 ft/sec velocity error, the period of coherence of the LO must be longer than $1.77 \cdot 10^{-3}$ seconds. The resulting phase error in the beacon delay of 5.0 microseconds is

$$\text{Phase error} = \sqrt{\text{Beacon Delay/Period of Coherence}}$$
$$= \sqrt{5 \cdot 10^{-6}/1.77 \times 10^{-3}} = \sqrt{.283 \cdot 10^{-2}} = 0.0532 \text{ radians}$$
$$= 3.05 \text{ degrees} \tag{23}$$

10. **Frequency Stability: Output frequency must be within + 0.125 cps of input frequency**

The Doppler equivalent of a 0.01 ft/sec change in velocity (see Appendix I).

11. **Recovery Time: 25 Microseconds**

See Appendix J.

12. **Peak Power Output: 4.0 watts (250 mile range); 400 watts (2500 mile range); based on use with AN/FPS-16 radar modified for 2.4 microsecond pulse.**

The required power output from the coherent beacon, P_b, is given by

$$P_b = P_r \cdot \frac{(4\pi R)^2}{G\lambda^2} \tag{21}$$

where P_r, is the minimum useful received signal, R is range, G is radar antenna gain, and λ is wavelength; an omni-directional beacon antenna is assumed. The minimum useful received signal may be calculated from

$$P_r = (S/N)_{min} \cdot N \cdot (NF) \times L_R \times L_B$$

$$= (S/N)_{min} \cdot kTB \cdot (NF) \times L_R \times L_B \qquad (22)$$

where $(S/N)_{min}$ = minimum useful S/N ratio; taken as 6 db, $N = kTB = $

receiver noise; k = Boltzman's constant, $1.38 \cdot 10^{23}$; T= absolute temper-

ature, taken as $300^{\circ}K$; B = radar receiver bandwidth, taken as 0.4 Mc

(reciprocal of 2.4 microsecond pulse width); NF = radar receiver noise

figure, taken as 8 db; L_R = radar receiving losses, taken as 2 db; L_B =

beacon transmitting losses, taken as 2 db. The resulting value of P_r is

$$P_r = 1.0 \times 10^{-13} = -100 \text{ dbm}$$

For an antenna gain of the AN/FPS-16 of 44 db, a wavelength of

2 in, and a range of 250 miles (required on high altitude shots at WSMR),

the power required from the beacon is

$$P_b = P_r \frac{(4 \pi R)^2}{G \lambda^2} = 0.04 \text{ watts.}$$

Allowing 20 db for missile antenna nulls gives a beacon power requirement

of 40 watts. A power output of 400 watts would increase the maximum range

to 2500 miles.

B. Varactor Tuned Tunnel Diode Oscillators

1. Introduction

During the past quarterly period the study of varactor tuned tunnel diode oscillators at C-Band has continued. This section considers the theory of operation of such devices and presents initial data on tuning range and power output of an experimental model.

2. Theory

The theory of tunnel diode oscillators has been reported extensively in the literature. Haneman and Thomson have presented a semi-quantitative analysis of the varactor tuned oscillator.[4] They report a tuning range from an operating frequency of 600 Mc to 900 Mc. In this section the theory governing the operation of an idealized model is presented. The model shown in Figure 6 was chosen for the purpose of this study. It consists of a length of transmission line terminated at opposite ends by a tunnel diode and a varactor diode. A high impedance shorted stub is in shunt with the varactor to provide a dc return for the biasing networks required.

In order to simplify the analysis it will be assumed that the resistance coupled into the network by the output is lumed into R_S. Then

$$Z_{IN} = R_{IN} + j X_{IN} \tag{24}$$

where

$$R_{IN} = \frac{R}{1 - \dfrac{X}{Z_o}} \left\{ \frac{1 + \dfrac{X/Z_o \tan \beta \ell}{1 - X/Z_o} \tan \beta \ell}{1 + \left[\dfrac{R/Z_o \tan \beta \ell}{1 - X/Z_o \tan \beta \ell} \right]^2} \right\} \tag{25}$$
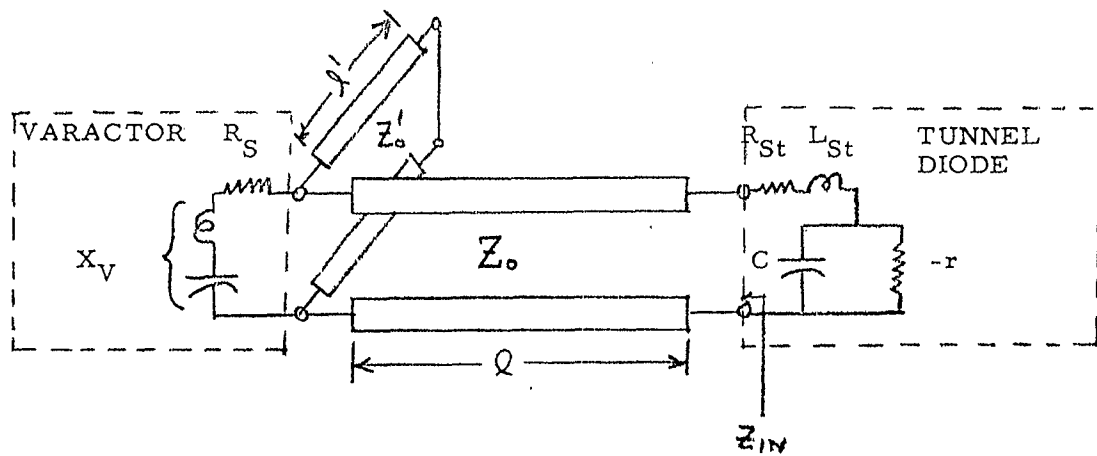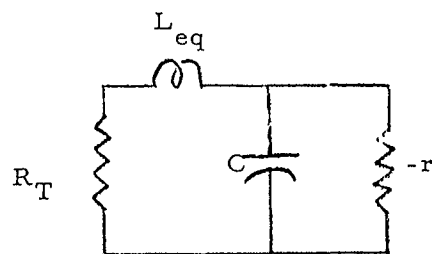
FIGURE 6 : VARACTOR TUNED OSCILLATOR

FIGURE 7 : OSCILLATOR EQUIVALENT CIRCUIT

27

$$X_{IN} = \frac{R}{1 - \dfrac{X}{Z_o}} \left\{ \frac{\dfrac{X/Z_o + \tan\beta\ell}{R/Z_o} - \dfrac{R/Z_o \tan\beta\ell}{1 - X/Z_o \tan\beta\ell}}{1 + \left[\dfrac{R/Z_o \tan\beta\ell}{1 - \dfrac{X}{Z_o}\tan\beta\ell} \right]^2} \right\} \tag{26}$$

$$R = \frac{R_S (Z_o' \tan\beta\ell')^2}{R_S^2 + (X_V + Z_o' \tan\beta\ell')^2} \tag{27}$$

$$X = \frac{R_S^2 Z_o' \tan\beta\ell' + X_V Z_o' \tan\beta\ell' (X_V + Z_o' \tan\beta\ell')}{R_S^2 + (X_V + Z_o' \tan\beta\ell')^2} \tag{28}$$

The oscillator equivalent circuit now takes the form of Figure 7 . If L_{eq} is defined such that

$$L_{eq} = \frac{X_{IN}}{\omega} + L_S, \tag{29}$$

steady state oscillations will result when

$$r = \frac{L_{eq}}{R_T C} \tag{30}$$

at a frequency $\omega_o = \left\{ \dfrac{1}{L_{eq} C} \left[1 - \dfrac{R_T^2 C}{L_{eq}} \right] \right\}^{1/2}$ (31)

where

$$R_T = R_{IN} + R_{St} \tag{32}$$

From a theoretical point of view, the above equations may be used to select Z_o, Z_o', ℓ, ℓ', such that the maximum tuning range is obtained. Computer techniques could be used to obtain plots of r and ω_o as a function of the various circuit parameters. Such plots would be of considerable aid in

ARMOUR RESEARCH FOUNDATION OF ILLINOIS INSTITUTE OF TECHNOLOGY

selecting the proper diodes.

A second model which warrants further attention is shown in Figure 8 . This model is somewhat more flexible and lends itself better to synthesis techniques. By restricting Y_{IN} to conform to the conditions required for steady state oscillation, it may be possible to establish optimum design criteria. Work will begin shortly along these lines.
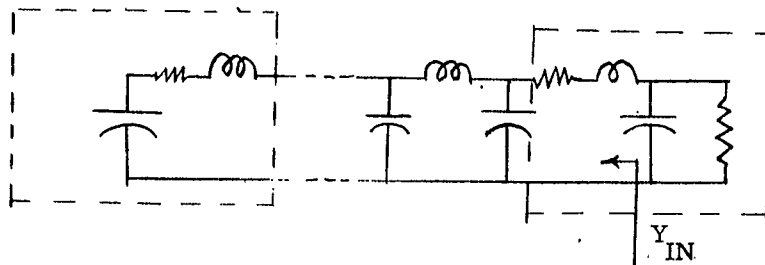
FIG 8 : MODEL TWO OF VARACTOR TUNED OSCILLATOR

3. Experimental Results

The experimental model which was fabricated during this quarterly period closely resembles the circuit shown in Figure 6 . The model design was based on strip transmission line techniques. A sliding wall was used to make Z_o variable while ℓ was fixed at approximately 1 inch. A sliding short was used to make ℓ' variable with Z_o' essentially fixed. The biasing circuit was simply a 16 ohm carbon type resistor in shunt with an r-f by pass. Various problems resulted from use of such a simple bias arrangement. These will be discussed in detail below. An MS1102 tunnel diode was used in conjunction with MA4254 varactor diode.

By properly adjusting Z_o and ℓ' the circuit could be made to oscillate at any frequency over the 5.0 kmc to 6.0 kmc band. Depending upon the adjustments, the oscillator could be electronically tuned over an 85 Mc to

200 Mc band. The varactor was always biased in the reverse direction. A

small amount of forward bias would increase the tuning range somewhat, but

this was not investigated.

A plot of power output, as determined by a spectrum analyzer, versus

frequency is shown in Figure 9 . This data was obtained for a fixed Z_o and

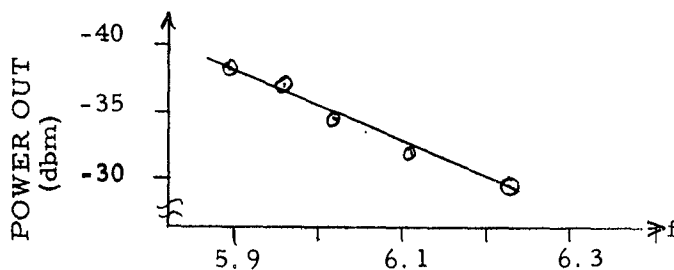λ ' and from 0 volts to near reverse breakdown bias on the varactor diode.

FIG. 9 : POWER OUT VS. FREQUENCY

4. Magnetically Tuned Oscillator

Magnetic tuning of tunnel diode oscillators has recently been reported

by Kotzebue[5] . By using a yttrium iron garnet resonator, a tuning range from

2. 5 gc to 4. 0 gc was obtained with a power output of the order or 60 μ watts.

For wide tuning range requirements magnetic tuning is obviously superior to

varactor tuning. However, for small tuning ranges such as is required in

beacon systems varactor tuning is simpler in the physical form of the circuit

required and less biasing power is necessary. For these reasons we believe

that varactor tuning warrants further effort.

5. Future Work

Further work on the tunnel diode biasing circuit is required to stablize

the oscillations. Adjustment of the tunnel diode bias to obtain steady oscillation

was also tedious. The r-f by pass of both the varactor and tunnel diode indicated

a small amount of r-f leakage. The oscillation could be shifted slightly by making contact with the bias leads.

This model was developed primarily to indicate feasibility of varactor tuning at C-Band. As such the mechanical tuning adjustments were rather crude. A second model is now being designed which will incorporate a more elaborate biasing circuit and more precision mechanical adjustments. An applicable higher peak current tunnel diode is also being sought to increase the output power of the oscillator. The final model will also be used as a basis for down-convertor investigations.

As mentioned previously sysnthesis work on the oscillator model shown in Figure 8   will commence shortly.

C. Analysis and Design of a New Tunnel Diode Biasing Circuit

1. General Discussion

As it was mentioned in the Second Quarterly Report, because of "burnout" problems that occurred when biasing high cut-off frequency tunnel diodes, the biasing circuit had to be modified considerably. It was determined experimentally that "burnout" is due to the following factors:

a) improper grounding of instruments used in testing the device,

b) transcients due to power line,

c) strong dc or ac signals generating in instruments used (such as battery operated voltmeters and spectrum analyzers),

d) strong RF signals existing in the vicinity of the device (such as radar signals),

e) poor connections in the dc biasing circuit,

f) strong electrostatic pick-up.

The following steps were taken to eliminate the above problems, respectively:

a) all instruments were connected to the same ground, but disconnected from the ground of the power line,

b) a germanium semiconductor diode was used (see Figure10) so that the voltage across the tunnel diode could not exceet 0.7v; at 0.7v this diode conducts very strongly,

c) VTVM voltmeters were used instead of direct voltmeters; also proper isolation was used in using spectrum analyzers or other instruments with high RF leakage,

d) large high frequency by-passing capacitors (see Figure 10) were utilized in conjunction with the above germanium diode,

e) the biasing circuit was carefully redesigned to avoid poor

connections,

f) it was found that electrostatic pick-up was considerably reduced

using the above mentioned by-passing capacitors (120 μF). This,

of course, is an additional precaution since the germanium diode

would be sufficient.

Taking the above precausionary steps, it was found that no "burnout"

problems occurred under any circumstances whatsoever. However, an

additional difficulty was observed as far as amplification of the tunnel diode

is concerned. Although high power gains were obtained, the amplification

was non-linear. This was due to the instability of the device and as a result

the I-V curve of the tunnel diode was highly distorted, (see Figure 14).

Because of this distortion, amplification was very critical to slight changes in

the position of the tuning adjustments. In addition, the distortion of the I-V

curve was a strong function of small changes of the input signal level and signal

frequency. These observations were possible by building a curve tracer in the

amplifier itself. More will be said about stability and non-linear amplification

in the following sections.

2. Stability of Biasing Circuit

As stated above, instability in the biasing circuit causes distortion

in the I-V characteristic curve of a tunnel diode, and as a result its equivalent

circuit parameters change considerably with frequency of oscillation and amount

of external loading. But to establish accurate design criteria for a C-Band

tunnel diode amplifier, it would be necessary to obtain first a smooth, undistorted

I-V tunnel diode characteristic curve. To accomplish this, the following analysis

of the biasing circuit is presented based on the Niguist criterion, which happens

to be more practical and convenient in this case than the Routh-Hurwitz criterion. The circuit to be analyzed is that of Figure 10. This equivalent circuit can be simplified considerably by first examining the plot of $\dot{Z}_{TD}$ $(j\omega)$ in Figure 12 at low frequencies. Since C_1 is large enough to cancel out any lead inductances (L_1) in the circuit, it is readily seen that the circuit to the left of the transmission line can be replaced by an equivalent resistive load R'_L. After making the above approximation, the circuit of Figure 10 becomes that of Figure 11 which is certainly much easier to analyze.

From Figure

$$Z_i(\theta) = Z_o \left[\frac{R'_L + j Z_o \tan \theta}{Z_o + j R'_L \tan \theta} \right] \tag{33}$$

$$= \frac{Z_o \left[R'_L Z_o (1 + \tan^2 \theta) + j (Z_o^2 - R'^2_L) \tan \theta \right]}{Z_o^2 + R'^2_L \tan^2 \theta}$$

where

$$\theta = \frac{2\pi \ell}{\lambda}$$

λ = free-space wavelength,

ℓ = length of line,

Z_o = characteristic impedance of line.

From Equation (33)

$$R_i(\theta) = \frac{Z_o^2 R'_L (1 + \tan^2 \theta)}{Z_o^2 + R'^2_L \tan^2 \theta} \tag{34}$$

$$X_i(\theta) = \frac{Z_0(Z_0^2 - R_L'^2)\tan\theta}{Z_0^2 + R_L'^2 \tan^2\theta} \tag{35}$$

where

$$Z_i(\theta) = R_i(\theta) + j X_i(\theta)$$

also

$$Z_{TD}(S) = \frac{L_S C S^2 + (R_S C - L_S/r) S + (1 - R_S/r)}{C S - \dfrac{1}{r}} \tag{36}$$

and for $S = j\omega$

$$Z_{TD}(j\omega) = \left[R_S - \frac{r}{1 + (\omega r C)^2}\right] + j\omega\left[L_S - \frac{C r^2}{1 + (\omega r C)^2}\right] \tag{37}$$

Then the total loop impedance would be

$$Z_T(j\omega) = Z_i(j\omega) + Z_{TD}(j\omega) \tag{38}$$

It must be noticed, from Equation (36), that the tunnel diode impedance $Z_{TD}(S)$ has a single pole in the RHP of the S-plane.

Now, according to the Nyquist criterion, and knowing that $Z_{TD}(S)$ has one pole in the RHP, the locus of $Z_T(j\omega)$ must encircle the origin once in the positive (counter clockwise) direction as the frequency increases from $-\infty$ to $+\infty$. If this condition holds the circuit of Figure 11 would be stable.

In general, at the self resonant frequency,

$$X_{TD}(\omega_{ox}) = 0$$

then

$$R_{TD}(\omega_{ox}) = R_S - \frac{L_S}{rC} \tag{39}$$

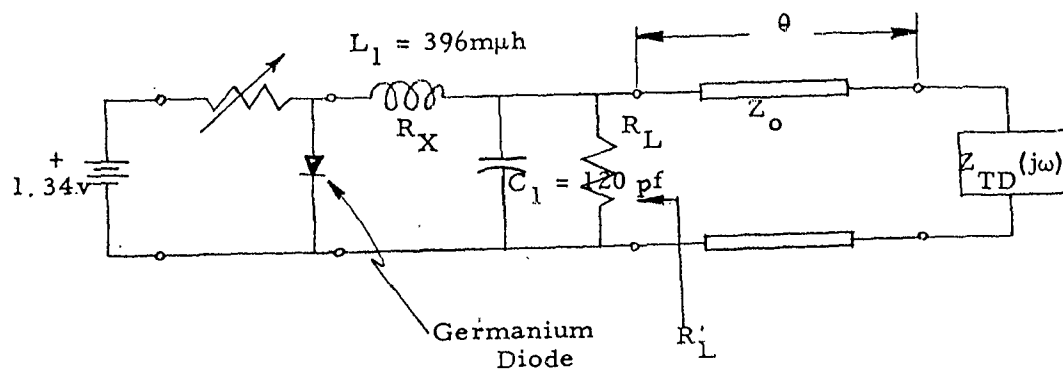In Figure 12, $Z_{TD}(j\omega)$ is plotted for a Sylvania D4168D tunnel diode. For

FIG. 10 BIASING CIRCUIT OF A TUNNEL DIODE AMPLIFIER
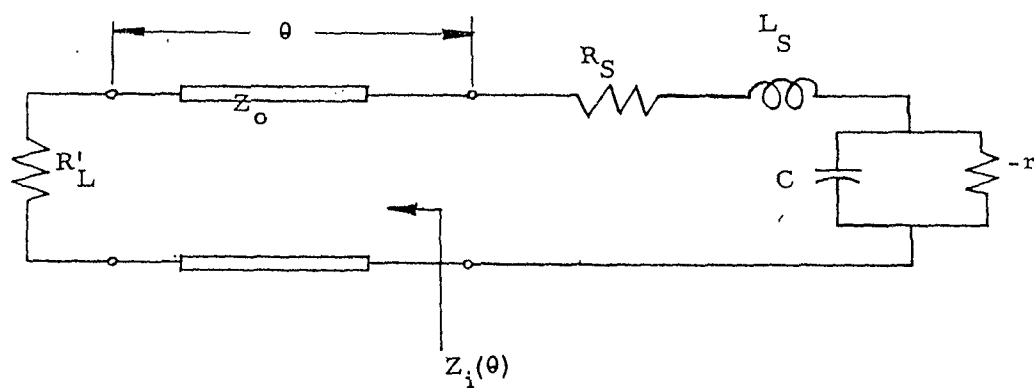

FIG. 11   SIMPLIFIED BIASING CIRCUIT OF A TUNNEL DIODE
AMPLIFIER

FIG. 12 NYQUIST PLOTS OF Z_{TD} AND Z_T ILLUSTRATING STABILITY CRITERIA

Type of Tunnel Diode Used: D4168D

$-r = -78\ \Omega$

$R_S = 2.5\ \Omega$

$C = 0.46$ pf

$L_S = 0.3\ m\mu h$

$Z_{TD}\ (j\omega)$

$Z_T\ (j\omega)$

$\left.\begin{array}{l} Z_o = 8\ \Omega \\ R_L' = 2\ \Omega \end{array}\right\} B$

$\left.\begin{array}{l} Z_o = 8\ \Omega \\ R_L = 4\ \Omega \end{array}\right\} A$

$\varepsilon = 0$

$\varepsilon = \infty$

$+j\ X$

$+R$

37

this diode,

$$f_{ox} = 11 \text{ kmc}$$

and

$$R_{TD} (\omega_{ox}) = -8.5 \ \Omega \tag{40}$$

Now, for stable operation,

$$R_{TD} (\omega_{ox}) < R_i (\theta_{ox}) \tag{41}$$

and

$$X_i (\theta_{ox}) = 0 \tag{42}$$

By applying conditions (41) and (42), the curve of $Z_{TD} (j\omega)$ in Figure 12 would shift to the right and thus encircle the origin once. Also condition (42) implies that the coaxial line must be a quarter wavelength long at 11 kmc or at the self resonant frequency of the tunnel diode. In Figure 12, two curves of $Z_T (j\omega)$ were plotted for different combinations of R_L' and Z_o. It is seen that curve A is stable whereas curve B is not. Curve B clearly indicates that conditions (41) and (42) are not sufficient for stability. For this reason, a cut-and-try procedure is needed to obtain Nyquist criterion. In addition it must be noticed that the biasing circuit impedance has a considerable effect on the tunnel diode impedance, especially around the self resonant frequency, which must be taken into account when designing microwave tunnel diode amplifiers; in fact, it would require lower impedance external circuitry.

3. Design and Experimental Investigation of the Biasing Circuit

The biasing circuit was actually designed using the combination

$$\left. \begin{array}{l} Z_o = 8 \ \Omega \\ \\ R_L' = 4 \ \Omega \end{array} \right\}$$

which as seen from Figure 12 , represents a stable condition. Finally,
a curve tracer was built in the RF circuit to check the I-V characteristic
curve of the tunnel diode. It was found experimentally that a disc carbon
resistor of 16 Ω (see Figure 13) is needed to obtain stable operation.
It would seem that a 16 Ω disc carbon resistor gives an $R_L' = 4\Omega$ in
Figure 11 . Figure 16 show   photograph of the I-V curve of a Sylvania
D4168D type tunnel diode, while Figure 14 shows an I-V distorted curve
when a 25 Ω disc carbon resistor was used in the biasing circuit; this
distortion, of course, is due to oscillations in the amplifier. It was also
noticed that the stability of the circuit was not affected by changing the
position of sliding shorts used in the device, see Figure 13 . The fact
that the amplifier is stable (by observing the I-V curve) regardless of the
position of tuning adjustments, makes it possible to tune the amplifier in
the frequency range of interest and establish accurate design criteria for
it at microwave frequencies.

Experimental work on amplifier performance using the new biasing
circuit will begin soon. During this third quarterly period some data was
taken using the biasing circuit described in the second quarterly report.
Figure 17 shows the insertion power gain of the amplifier versus frequency.
The maximum power gain that could be obtained in the frequency of interest
was 11.5 db. The 4 db bandwidth extended from 5.5 kmc to 6.27 kmc.
Although the response is quite satisfactory, it was highly critical to tuning
or small changes in the circuit. For this reason it was necessary to redesign
the biasing circuit and check it with a curve tracer built in the amplifier itself.
In addition, Figure 18 shows relative output power versus input power. It is
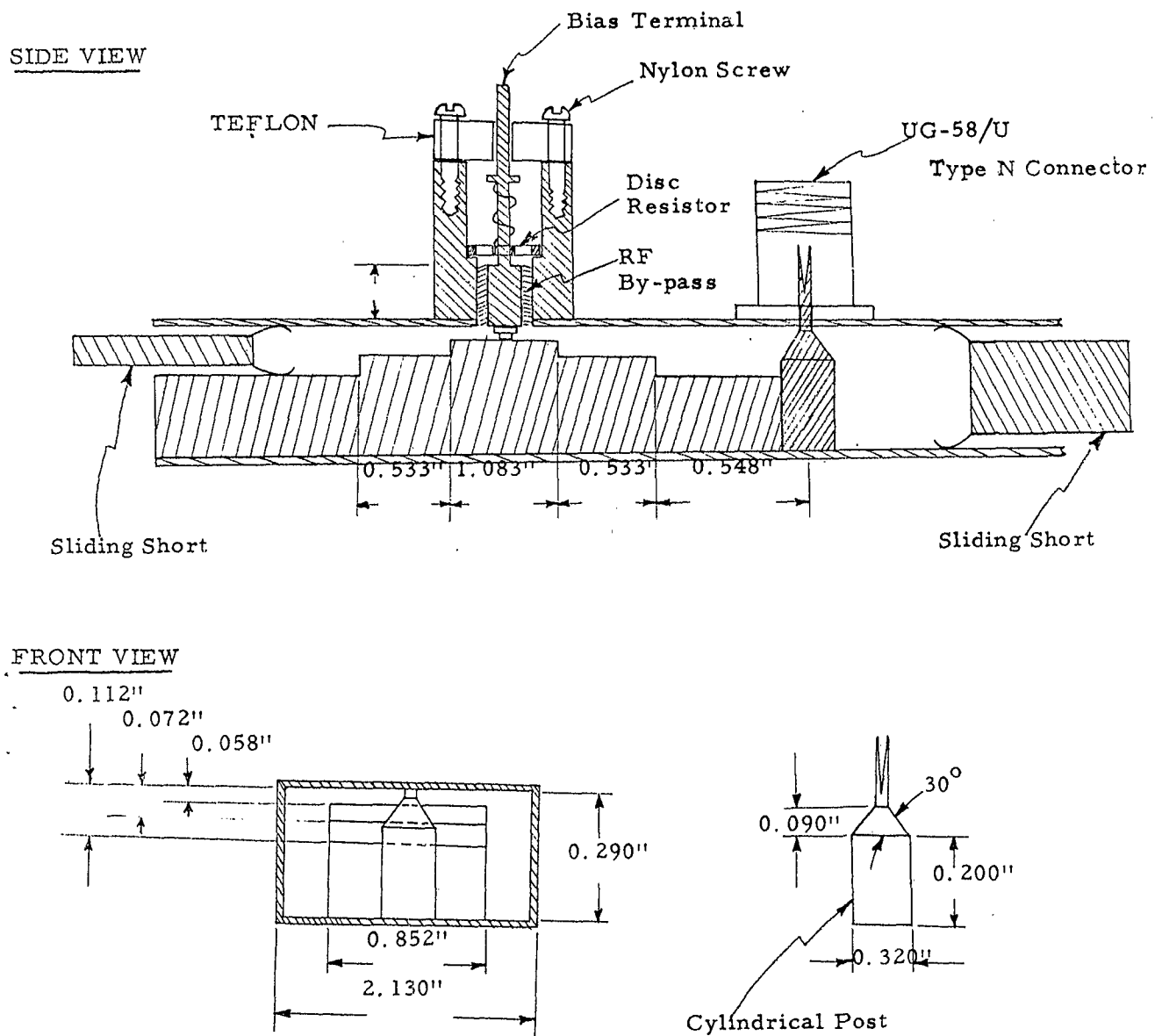seen that the amplifier is non-linear below -40 dkm of input power, indicating

SIDE VIEW

Bias Terminal

Nylon Screw

TEFLON

UG-58/U
Type N Connector

Disc
Resistor

RF
By-pass

0.533" 1.083" 0.533" 0.548"

Sliding Short

Sliding Short

FRONT VIEW

0.112"
0.072"
0.058"

0.290"

0.852"

2.130"

30°

0.090"

0.200"

0.320"

Cylindrical Post

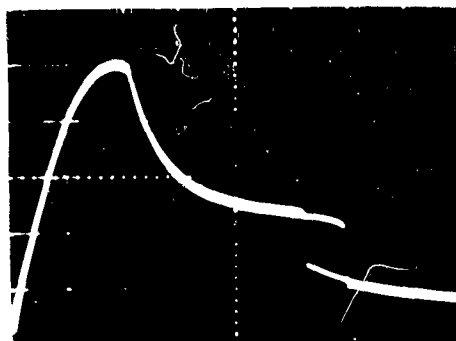FIG. 13 CROSS-SECTIONAL VIEW OF A RIDGED-WAVELENGTH C-BAND
TUNNEL DIODE AMPLIFIER

40

FIG. 14   I-V CURVE OF A STRONGLY OSCILLATING TUNNEL
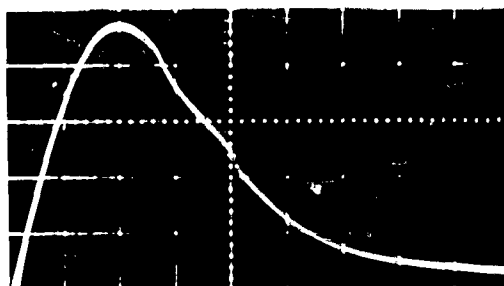DIODE (D4168D)

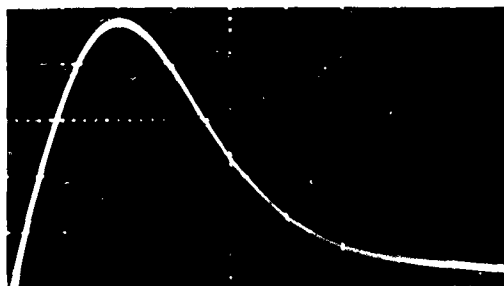FIG. 15   I-V CURVE OF AN OSCILLATING TUNNEL DIODE
(D4168D)

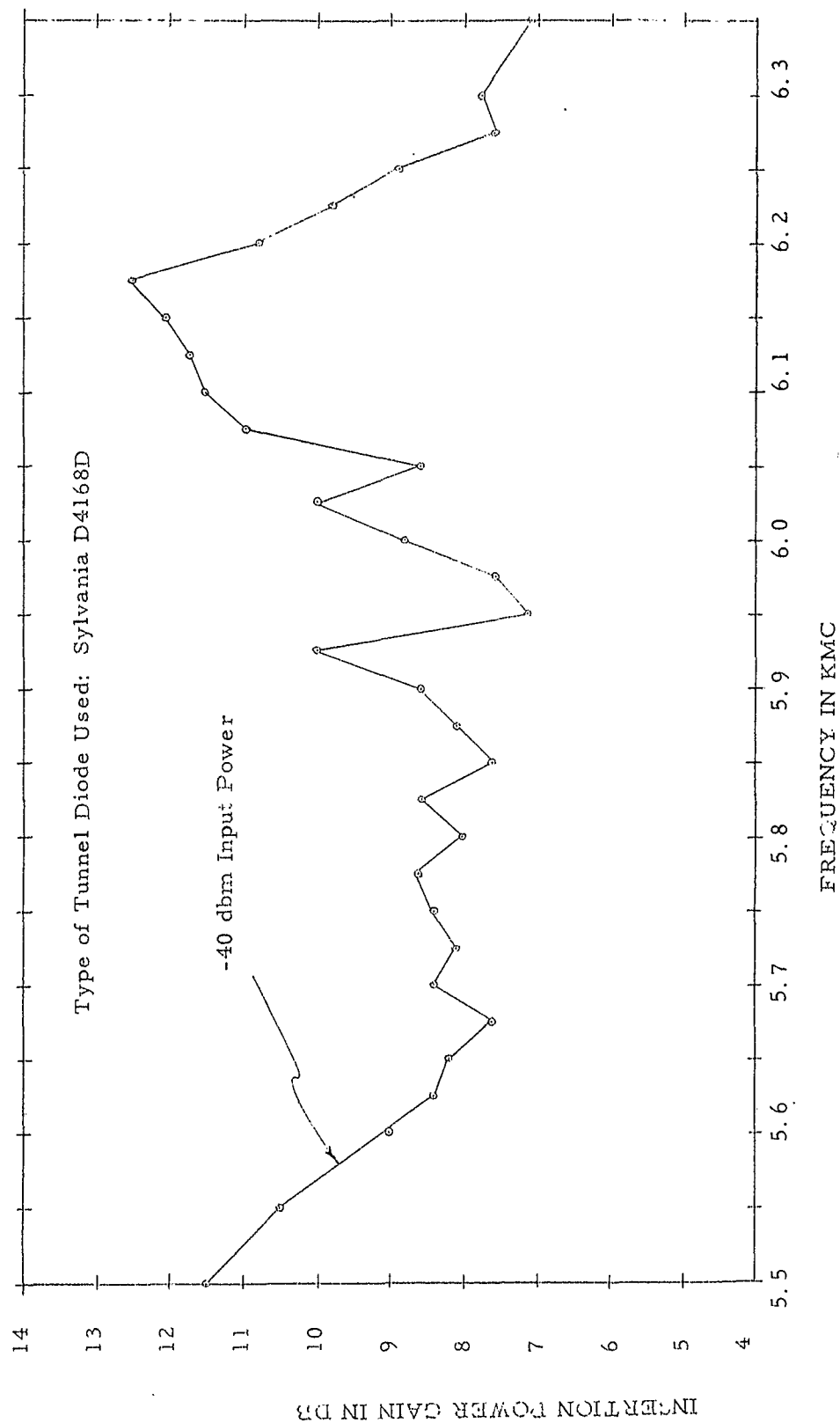FIG. 16   I-V CURVE OF A NON-OSCILLATING TUNNEL DIODE
(D4168D)

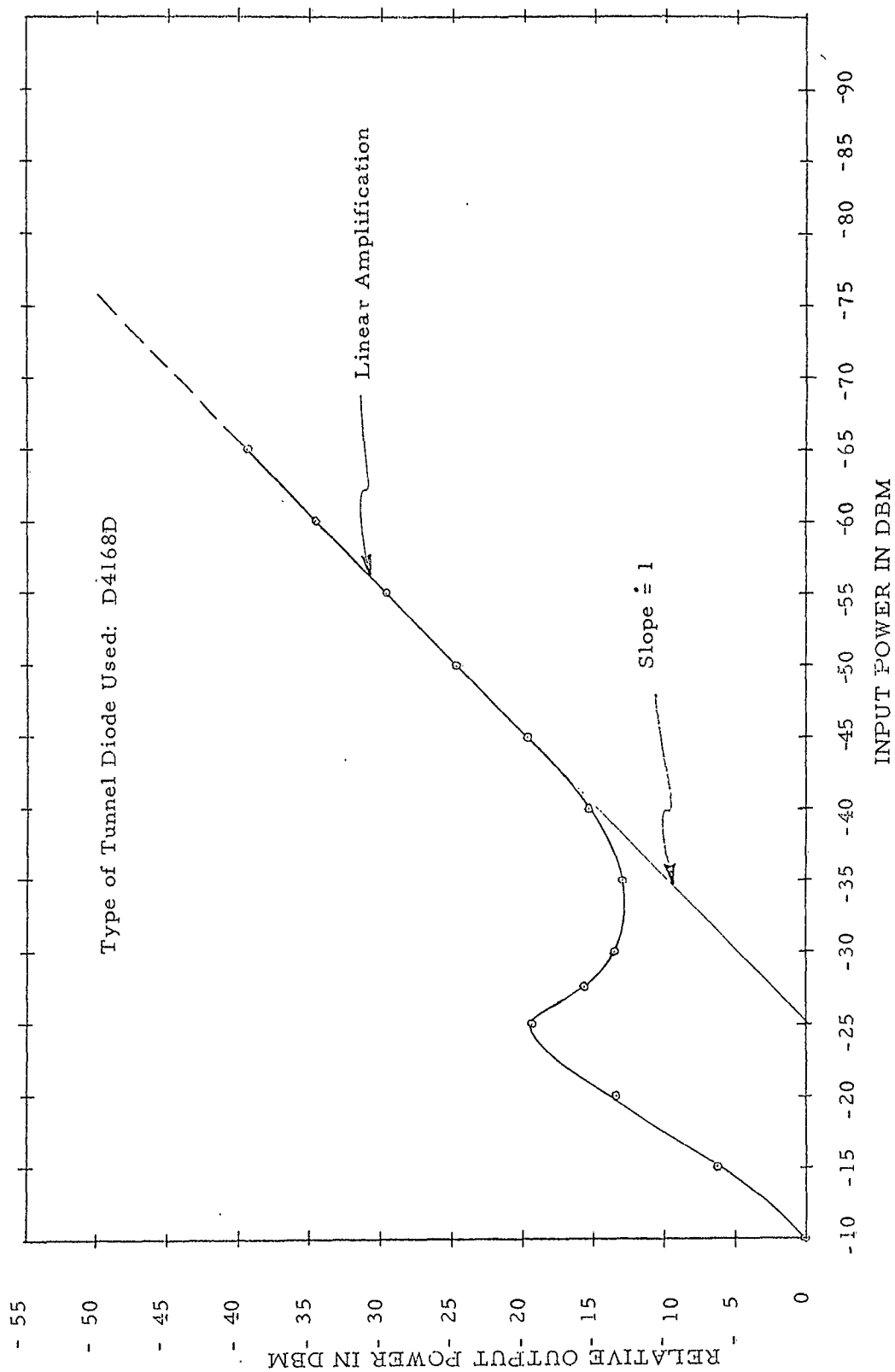FIG. 17 GAIN VERSUS FREQUENCY DIAGRAM OF TUNNEL DIODE AMPLIFIER

42

FIG. 13 DIAGRAM ILLUSTRATING RELATIVE OUTPUT POWER VERSUS INPUT POWER OF
TUNNEL DIODE AMPLIFIER

43

that the biasing circuit was oscillating at a frequency outside the range of 5.5 kmc to 6.27 kmc. It can be concluded, therefore, that the limiting phenomenon in tunnel diode amplifiers (this same phenomenon was observed in previous experiments) is due to oscillations at frequencies outside the band of interest. It is believed that by utilizing the above described biasing circuit it would be possible to obtain a linear tunnel diode amplifier down to at least -10 dkm input power.

III. CONCLUSIONS

Coherent Radar-Beacon Systems

1. A fundamental limitation on the accuracy of coherent radar-beacon systems is due to frequency instabilities in the radar transmitter and beacon-local-oscillator. Inaccuracy increases with increasing propagation delay, in the case of the radar, and with increasing beacon delay. At the present state of the art of stable oscillators, the errors introduced by the radar are larger, because of the larger delay. However, errors on the order of a few hundredths of foot/sec appear readily achievable.

2. Although velocity tracking accuracy is improved by coherent operation, the maximum range of the coherent system is normally limited by that of the range tracking loop which provides gating of the Doppler channel. Extension of range is possible by applying narrow-band filtering techniques to the Doppler channel, after normal range and Doppler tracking have been established. However, a serious acquisition problem may exist at extended ranges since a search in Doppler must be performed as well as in range.

3. Velocity accuracy improvement due to coherency will be less than

$$\left(\frac{1}{2} f_0 \tau \right)$$

by an amount depending on the type of target motion. Thus, for random steps of acceleration, the improvement is

ARMOUR RESEARCH FOUNDATION OF ILLINOIS INSTITUTE OF TECHNOLOGY

45

$$(\frac{1}{\sqrt{2}} f_o \tau)^{1/4}.$$

Coherent Beacon

1. A coherent beacon which is basically an amplifier, employing i-f conversion and delay, appears feasible. However, considerable work must be done to establish the capabilities of the techniques involved. Coherent beacon specifications, many of which can only be considered design goals, are presented in the body of the report.

Beacon Components

1. Varactor tuning of tunnel diode oscillators at C-Band has been shown to be feasible through work on an experimental model.

2. To obtain accurate design criteria for a c-band tunnel diode amplifier, it is necessary to have a stable dc biasing circuit. Otherwise, the amplifier is very critical to mechanical tuning. adjustments.

IV. PROGRAM FOR NEXT INTERVAL

Coherent Radar-Beacon Systems

The effect of beacon antenna rotation or tumbling in producing Doppler, (i. e. velocity) tracking errors will be analyzed.

Beacon Compnents

Model II of the varactor tuned oscillator will be designed having a more sophisticated biasing circuit and precision mechanical tuning adjustments. Following fabrication the device will be used in detection and down conversion studies.

Experimental work on the C-band tunnel diode amplifier will continue in an effort to improve its performance by designing several waveguide ridges and using the stable dc biasing, circuit described in this report.

V. IDENTIFICATION OF PERSONNEL

The following personnel have contributed to work herein reported during the past quarterly:

J. T. Ludwig, Manager
Antennas, Microwaves, and Propagation
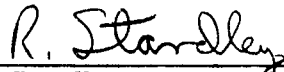
S. Kazel, Research Engineer

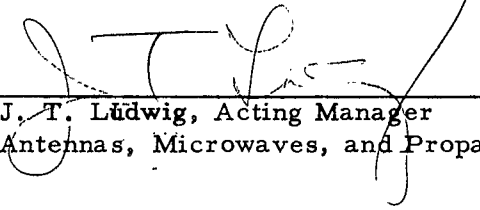R. Standley, Research Engineer

P. Toulious, Assistant Engineer

J. Feldman, Assistant Engineer

Respectfully submitted,

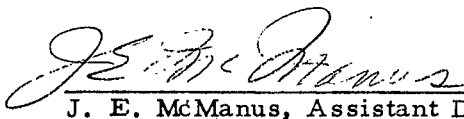ARMOUR RESEARCH FOUNDATION
of Illinois Institute of Technology

R. Standley, Research Engineer

J. T. Ludwig, Acting Manager
Antennas, Microwaves, and Propagation

APPROVED:

J. E. McManus, Assistant Director
Electronics Research

REFERENCES

1. "Evaluation and Improvement of Radar-Beacon Systems," Final Report, 30 June 1961, Contract No. DA-36-039 SC-85318.

2. "Coherent Pulse Doppler Study Program," Final Report, 1 July 1961 - 30 June 1962, Contract No. DA 36-039 SC-87310, Radio Corporation of America, Moorestown, New Jersey.

3. "Mathematical Analysis of Random Noise," S. O. Rice, Bell System Technical Journal, Vol. 23 and Vol. 24.

4. F. Haneman and G. Thomson, "Varactor-Tuned Tunnel Diode Oscillator Now Practical," Electronics, pp. 50-52, Sept. 21, 1962.

5. K. Kotzebue, "A Wide-Range Electronically Tuned Tunnel Diode Microwave Oscillator," Proc. IEEE Vol. (51)3, pp. 488-489, March 1963.

APPENDIX A

SIGNAL-TO-NOISE IMPROVEMENT DUE TO COHERENCY

The effective (voltage) signal-to-noise improvement, R, of pulse-Doppler radar over (non-coherent) pulse radar is readily obtained from the analysis of a previous report.[1] The S/N improvement, R, should not be confused with the improvement factor, F, in velocity tracking accuracy derived in Ref. 1. S/N improvement is the <u>cause</u> of tracking accuracy improvement. S/N improvement is <u>independent</u> of the type of target motion (as will be shown here), whereas tracking accuracy improvement <u>depends</u> on the type of target motion (as shown in Ref. 1).

Case I: Random Steps of Velocity

(a) Pulse (Non-coherent) Radar:

$$(S/N)_p \sim \frac{\text{Signal power density}}{\text{Noise density}} \Big]_{\omega = 0} = \frac{\phi^2}{k^2}$$

$$= \frac{\frac{8}{\pi C^2} V^2_{rms}/K}{\tau^2 \eta / 3\pi P_{av}} = 24 \frac{V^2_{rms} P_{av}}{c^2 K \eta} \cdot \frac{1}{\tau^2}$$

(b) Pulse-Doppler

$$(S/N)_{pd} \sim \frac{\phi^2}{k^2} = \frac{\frac{8}{\pi C^2} f_o^2 V^2_{rms}/K}{\frac{2}{3\pi} \eta / P_{av}}$$

$$= 12 \frac{V^2_{rms} P_{av}}{c^2 K \eta} \cdot f_o^2$$

Taking the ratio of the above values of S/N power ratios gives R^2:

$$R^2 = \frac{(S/N)_{pd}}{(S/N)_p} = (1/2)f_o^2 \tau^2$$

or

$$R = \frac{1}{\sqrt{2}} f_o \tau$$

Case II: Random Steps of Acceleration.

(a) Pulse

$$(S/N)_p \sim \frac{\phi^2}{k^2} = \frac{\frac{8}{\pi C^2} a_{rms}^2/K}{\tau^2 \eta /3\pi P_{av}}$$

$$R^2 = \frac{(S/N)_{pd}}{(S/N)_p} = (1/2)f_o^2 \tau^2$$

$$R = \frac{1}{\sqrt{2}} f_o \tau$$

Thus the effective (voltage) signal-to-noise improvement, R, in the tracking loop is given by $\frac{1}{\sqrt{2}} f_o \tau$ (independent of type of target motion).

(b) Pulse-Doppler

$$(S/N)_{pd} \sim \frac{\phi^2}{k^2} = \frac{\frac{8}{\pi} f_o^2 a_{rms}^2/C^2 K}{\frac{2}{3\pi} \eta /P_{av}}$$

APPENDIX B

VELOCITY ACCURACY OF NON-COHERENT PULSE RADARS

Assume that the non-coherent radar obtains velocity, v, from

$$v = \frac{x_1 - x_2}{T}$$

where x_1 and x_2 are measured positions at the beginning and end of the time interval T. Assuming uncorrelated rms errors in position of magnitude, σ_p (before low pass filtering), the rms velocity error is

$$\sigma_v = \frac{\sqrt{2}}{T} \sigma_p$$

The effect of low-pass filtering is to reduce the error by a factor of [*]

$$\frac{1}{2} \sqrt{f_r / B}$$

where f_r = PRF and B = low-pass bandwidth, giving

$$\sigma_v = \frac{1}{\sqrt{2} T} \sqrt{f_r / B} \, \sigma_p$$

The rms error in position is given by

$$\sigma_p = \frac{1}{2} \frac{c \, \tau}{(V_s / V_n)}$$

where c = velocity of light, τ = pulse width, and V_s / V_n = input S/N ratio.

The smoothing time, T, and the low-pass bandwidth are related by

$$B = \frac{1}{2T}$$

[*] "Radar-Beacon System Study," Third Quarterly Progress Report, Contract DA-36-039 SC-73038.

ARMOUR RESEARCH FOUNDATION OF ILLINOIS INSTITUTE OF TECHNOLOGY

Combining the above gives the final expression for rms velocity error

$$\sigma_v = \frac{c\,\tau}{\sqrt{T^3 f_r}\,(V_s/V_n)}\ .$$

APPENDIX C

SIGNAL-TO-NOISE IMPROVEMENT DUE TO

BANDPASS FILTERING

For an i-f train of rectangular pulses of height V_s, pulse width τ, and period T, the carrier component, C, is

$$C = \frac{\tau}{T} V_s .$$

The original noise power density, η , is reduced in magnitude by gating to the value η':

$$\eta' = \frac{\tau}{T} \eta$$

where τ/T equals the gating factor. Thus, the S/N ratio, $(P_s/P_n)_{bp}$ after narrow band-pass filtering of the carrier component is

$$(P_s/P_n)_{bp} = \frac{C^2}{\eta' B_{bp}} = \frac{(\frac{\tau}{T} V_s)^2}{\eta \cdot \frac{\tau}{T} B_{bp}} = \frac{\tau}{T} \cdot \frac{V_s^2}{\eta B_{bp}}$$

where B = width of band-pass filter.

Since the i-f bandwidth, B_{if}, is given by

$$B_{if} = {}^1/\tau$$

and substituting $f_r = 1/_T$, we may write

$$(P_s/P_n)_{bp} = \frac{f_r}{B_{bp}} \frac{V_s^2}{B_{if} \eta}$$

But V_s^2 and $B_{if}\eta$ are the input signal and noise power, respectively, giving

$$(P_s/P_n)_{bp} = \frac{f_r}{B_{bp}} (P_s/P_n)_{if}$$

or $$(V_s/V_n)_{bp} = \sqrt{\frac{f_r}{B_{bp}}} (V_s/V_n)_{i-f.}$$

ARMOUR RESEARCH FOUNDATION OF ILLINOIS INSTITUTE OF TECHNOLOGY

APPENDIX D *

COMPARISON OF AN/FPS-16 AND

AN/FPQ-6 PARAMETERS

	AN/FPS-16	AN/FPQ-6
Antenna size	12 foot	29 ft. Cassegrainian
Antenna feed	4-horn monopulse	5-horn monopulse
Antenna beamwidth	1.2°	0.4°
Antenna gain	44 db	51 db
Antenna polarization	Vertical	Vertical, circular
Pedestal drive	Electric	Hydraulic
Antenna-pedestal rotation azimuth elevation	Continuous -10° to $+190^{\circ}$	Continuous -2° to 182°
Antenna-pedestal weight	16,000 lbs.	60,000 lbs.
Azimuth bearing	Ball	Hydrostatic
Angle-servo bandwidth	0.25 to 5 cps	0.5 to 5 cps
Angle-tracking rate-azimuth elevation	$40^{\circ}/sec$ $30^{\circ}/sec$	$28^{\circ}/sec$ $28^{\circ}/sec$
Angle-tracking percision	0.1 mil rms	0.05 mil rms
Frequency	5400-5900 Mc	5400-5900 Mc
Power output-fixed tunable	1 Mw 1/4 Mw	3 Mw
Pulse-repetition frequency	Various 341-1707 PPS	160-640 basic, 1707 max
Pulse duration	1/4, 1/2, 1 μsec	1/4, 1/2, 1 and 2.4 μsec
Pulse coding	Up to 5 pulses with duty cycle limits	Up to 5 pulses with duty cycle limits
Receiver noise figure	11 db	8 db
Receiver IF	30 Mc	30 Mc

ARMOUR RESEARCH FOUNDATION OF ILLINOIS INSTITUTE OF TECHNOLOGY

Receiver bandwidth	Switch with pulse width	1.2 to 1.6/pulse width
Receiver dynamic range	93 db with S.T.C.	110 db with programming
Range-tracking capability	500 nautical miles	32,000 nautical miles Continuous unambiguous
Tracking-range granularity	1 yard	2 yards
Acquisition features	Scan generator variable rep. rates	Scan generator Video integrator "C" scope and joy stick Pulse-coding capability "Aux-track" Multiple-gate array Digital-ranging system
Output - range	20-bit 2-speed binary, dc analog pot	25-bit single-speed binary
Output - angle	17-bit 2-speed binary 16:1 speed synchros Sine-cosine pots	19-bit binary with 8-bit dynamic lag correction 16:1 speed synchros Sine-cosine pots

---

* from "The Future of Pulse Radar", by D. Barton, IRE Transactions on Military Electronics, October, 1961.

APPENDIX E

PROBABILITY OF SUCCESSFUL INTERROGATION

Noise riding on the interrogation pulse may subtract from the signal, preventing the video pulse from triggering the threshold. The probability, P, of such pulse "cancellation" is given by

$$p = \frac{1}{2} \exp\left[-\frac{1}{2} \frac{(S-T)^2}{N^2}\right]$$

$$= \frac{1}{2} \exp\left[-\frac{1}{2} \left(\frac{S}{N} - \frac{T}{N}\right)^2\right]$$

For the previously calculated threshold-to-noise ratio, $T/N = 4.26$ (12.6 db) for 10 noise firings/sec., we may write

$$p = \frac{1}{2} \exp\left[-\frac{1}{2} \left(\frac{S}{N} - 4.26\right)^2\right]$$

The probability of pulse "cancellation", p, is tabulated below for various video signal-to-noise ratios, along with the percentage of successful interrogations, $100 \times (1-p)$.

Video Signal-to-Noise Ratio, S/N	Probability of Pulse Cancellation, p	Percent Successful Interrogations 100(1-p)
13.0 db	.49	51%
15.0	.20	80.
16.0	.062	93.8
17.0	.0095	99.1
18.0	.0005	99.95

Thus, to achieve 99.95% reliable triggering with 10 noise firings/sec requires a video signal-to-noise ratio of 18 db. In addition, noise "blooming" during the pulse, which had not been taken into account will require an additional 2 db of signal level, giving a required S/N ratio of 20 db.

APPENDIX F
NOISE REDUCTION DUE TO NARROW-BAND VIDEO FILTERING

L   Let N^2 be the noise power in the i-f bandwidth, B_{if}. The detected

envelope (linearly detected) will be Rayleigh distributed, with an envelope,

or video, power of $2N^2$. The total video power is divided between a DC power

component, $1.56N^2$, which is blocked, and an AC, or noise, power of $0.44N^2$.

The AC, or noise, power has a triangular power spectrum, as shown in

Fig. F-1. A low-pass filter will pass the shaded fraction of the noise power.

The noise power, $(P_N)_{vid}$ in the low-pass band, B_{vid}, is

$$(P_N)_{vid} = 0.88 \ N^2 \ \frac{B_{vid}}{B_{if}}$$

For a 6 mc i-f bandwidth, and a 200 kc video bandwidth (based on

a 2.4 microsecond pulse), the video noise power is

$$(P_N)_{vid} = 0.0295 \ N^2$$

corresponding to a noise reduction of 15.3 db, over the noise power, N^2,

in the i-f bandwidth.
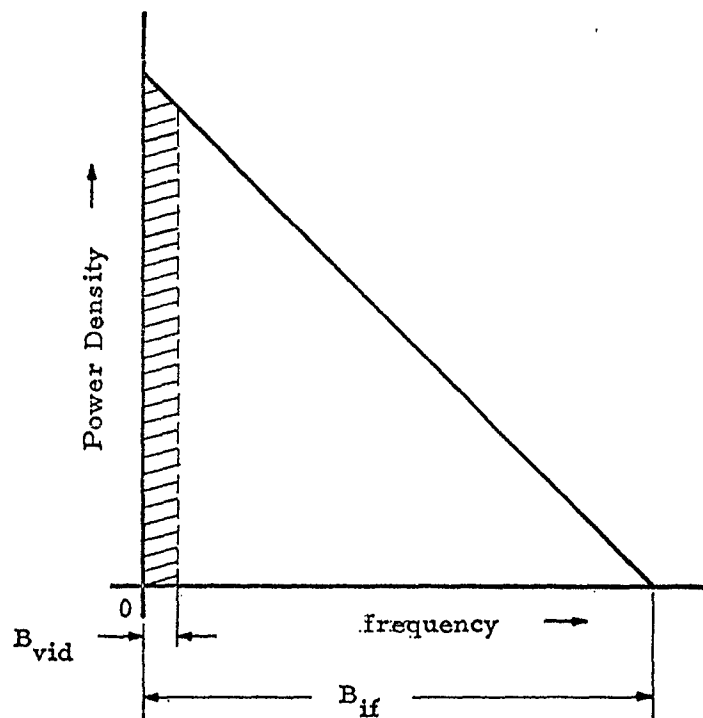
FIG. F-1 NOISE REDUCTION DUE TO NARROW-
BAND VIDEO FILTERING

F-2

APPENDIX G

TABULATION OF I-F AND CORRESPONDING VIDEO S/N RATIOS

IF S/N Ratio	Wideband Video[*] S/N Ratio	Narrow-band Video[**] S/N Ratio
0 db	-0. 6 db	13. 9
2	+3. 0	17. 5
3	+4. 5	19. 0
4	+6. 0	20. 5
6	+8. 5	23. 0

---

[*]Video signal-to-interpulse noise ratio.

[**]After narrow-banding improvement of 14. 5 db (Appendix F).

APPENDIX H

COHERENT BEACON SENSITIVITY CALCULATION

The false firing rate (noise firing rate) for Gaussian low-pass noise is given by

$$\frac{B}{\sqrt{3}} \exp\left[-\frac{1}{2}(T/N)^2\right]$$

where B is the low-pass bandwidth, T is the threshold level, and N is the rms noise. For B=200 kc, and a false firing rate of 10/sec, the corresponding threshold-to-noise ratio is found to be

$$T/N = 4.26 \text{ or } 12.6 \text{ db}$$

From Appendix E, for T/N = 13 db, the required video S/N ratio for 99.95 percent successful interrogation is

$$(S/N)_{video} = 18.0 \text{ db} + 2.0 \text{ db (for blooming)}$$
$$= 20 \text{ db}$$

From Appendix F, the 200 kc bandwidth video noise power is 15.3 db less than the unfiltered video noise power, giving a video detector output S/N ratio of

$$(S/N)_{detector} = 20.0 - 15.3 = 4.7 \text{ db}$$

From Appendix G, which tabulates output vs. input S/N ratio for a linear detector, the input, or i-f, S/N ratio corresponding to an output (S/N) ratio of 4.7 db is approximately

$$(S/N)_{i-f} = 3.0 \text{ db}$$

Thus the i-f S/N ratio for the minimum triggering signal is only 3.0 db. (Operation at such a low i-f S/N ratio is, of course, only possible because of the narrow-banding in the video.)

ARMOUR RESEARCH FOUNDATION OF ILLINOIS INSTITUTE OF TECHNOLOGY

It may appear that a beacon reply with only a 3.0 db S/N ratio is a poor signal to present to the tracking radar. However, the noise occupies a 6 mc band, while the signal band is only about 400 kc. The 700 kc i-f bandwidth of the AN/FPQ-6 will consequently improve the S/N ratio by 9.4 db to the value 12.3 db.

The noise power, n^2, is given by

$$n^2 = kTB \cdot (NF)$$

where k = Boltzmann's constant = $1.38 \cdot 10^{-23}$, T = reference temperature for noise figure = $300^\circ K$, B = i-f bandwidth, taken as 6.0 mc, and NF = noise figure, taken as 8 db for a crystal mixer input. The resulting noise power is

$$n^2 = 1.56 \cdot 10^{-13} \text{ watts} = -128 \text{ db} = -98 \text{ dbm}$$

Assuming a loss of 0.5 db in the circulator, 1 db in the diode switch, 2.5 db in the preselector, and a minimum i-f S/N ratio of 3.0 db as calculated above, the sensitivity, S, of the beacon is

$$S = -98 + 0.5 + 1.0 + 2.5 + 3.0 = -91 \text{ dbm}$$

For a tunnel diode input, with 5 db noise figure, the sensitivity would be -94 dbm.

APPENDIX I

LOCAL-OSCILLATOR STABILITY REQUIREMENTS

Random Errors

In the coherent beacon, the same LO is used, first, in mixing the input microwave pulse down to i-f, and later, in mixing the i-f pulse back up to its original frequency. Let the phase of the input be given by

$$(\omega_o t + \phi_o) \tag{1}$$

and let the phase of the LO be given by

$$\omega_1 t + \phi_1 + \Delta\phi(t) \tag{2}$$

where $\Delta\phi(t)$ represents phase variations due to frequency instabilities in the local-oscillator. The first mixing subtracts the LO phase from (1), giving

$$\omega_{if} t + \phi_o - \phi_1 - \Delta\phi(t) \tag{3}$$

where $\omega_{if} = \omega_o - \omega_1$. The second mixing, τ seconds later,

adds the LO phase,

$$\omega_1 (t + \tau) + \phi_1 + \Delta\phi (t + \tau) \quad , \tag{4}$$

to the i-f phase of (3), giving

$$(\omega_o t + \phi_o) + \omega_1 \tau + \left[\phi(t + \tau) - \Delta\phi(t) \right] \tag{5}$$

Thus, in addition to reproducing the input phase, $\omega_o t + \phi_o$, the output contains a fixed phase shift, $\omega_1 \tau$, and a random phase error, $\left[\Delta\phi(t + \tau) - \Delta\phi(t) \right]$. The fixed phase error is of no importance since only a changing phase can produce Doppler errors. The random phase error is the change in oscillator phase in the delay interval, τ. The mangitude of this error will change randomly from pulse to pulse (with an r.m.s. deviation), and will produce errors in the Doppler measurement.

ARMOUR RESEARCH FOUNDATION OF ILLINOIS INSTITUTE OF TECHNOLOGY

The above situation is exactly analogous to the effect of frequency instability in the coherent radar transmitter analyzed in the First Quarterly Report.[*] In that case, the time delay, τ, represented the two-way propagation delay. In the present case, τ, represents the beacon delay. Thus, Equation (28) of the First Quarterly Report may be used unchanged to obtain the r.m.s. velocity error $(\Delta v)_{rms}$, due to LO instability:

$$(\Delta v)_{rms} = \frac{1}{\sqrt{2}} \frac{c}{\omega T} \sqrt{\tau/T_c}$$

(6)

$$= \frac{1}{2\sqrt{2\pi}} \frac{\lambda}{T} \sqrt{\tau/T_c}, \quad \tau < T$$

where c = velocity of light, ω = r.f. frequency (radians/sec), T = smoothing time, τ = beacon delay, and T_c = period of coherence of beacon LO. Equation (6) may be solved for the period of coherence, T_c, giving

$$T_c = \frac{\tau}{8\pi} \left(\frac{\lambda}{\Delta v_{rms} T} \right)^2$$

(7)

The required value of T_c will be calculated for the following parameters:

τ = 5.0 μsec

λ = 5.3 cm = 2.0 in = 1/6 ft.

T = 0.1 sec

Δv_{rms} = 0.01 ft/sec.

The result is

$$T_c = 1.77 \times 10^{-3} \text{ sec.}$$

The corresponding spectrum width of the LO, $\delta\omega$, is

$$\delta\omega = \frac{1}{T_c} = 565 \text{ cps}$$

For a velocity error, Δv_{rms} = 0.1 ft/sec, the required spectrum width is 56,500 cps.

Frequency Drift

In addition to random frequency errors due to noise sources within the LO, frequency drift may occur due to changes in temperature, aging of components, etc. Any frequency drift, df, during the beacon delay time, will cause an error of the same amount in the Doppler measurement. The Doppler shift relationship is

$$f_d = 2 \frac{v}{\lambda}$$

or

$$d_{f_d} = 2 \frac{dv}{\lambda}$$

Setting df_d = df gives the velocity error due to the change in LO frequency:

$$dv = \frac{\lambda}{2} df$$

The allowable frequency drift during the beacon delay interval for dv = 0.01 ft/sec, and λ = 1/6 ft, is

$$df = \frac{2}{\lambda} dv = \frac{2}{1/6} 0.01 = 0.12 \text{ cps}$$

APPENDIX J

EFFECT OF MUTUAL INTERFERENCE AMONG SEVERAL

RADARS ON COHERENT BEACON PERFORMANCE

Missing Pulses

When several radars are simultaneously interrogating a beacon, mutual

interference occurs through the phenomena of beacon recovery time. Missing

pulses will result for each radar, causing noise in the Doppler tracking loop

and, consequently, velocity errors. In order to establish the requirements on

recovery time for a coherent beacon, the effect of missing pulses on S/N ratio

is now derived.

The noise power, V_n^2, due to missing pulses in a video pulse train,

as shown by Kretzmer[1], and presented in a previous report[2], may be written

$$V_n^2 = 2A^2 D^2 \frac{f_a}{f_r} F (1 - F)$$ (1)

where A = pulse height, D = duty ratio, f_r = PRF, f_a = low-pass bandwidth

(assumed much less than f_r), and F = fraction of missing pulses.

An r-f (or i-f) pulse train with missing pulses may be viewed as a

c-w carrier, A-M modulated by the above video pulse train. Since A-M

modulation spreads the modulation power equally on both sides of the carrier

(i. e., upper and lower sidebands), it follows that the noise power density is

reduced by a factor of two for the r-f pulse train. Thus the noise power, V_n^2,

appearing in an r-f pass band, f_{bp}, centered on the carrier frequency, is

[1] E. R. Kretzmer, "Interference Characteristics of Pulse-Time Modulation",
   M. I. T. Research Laboratory of Electronics, Technical Report No. 92 , May
   27, 1949.

[2] "Radar-Beacon System Study", Third Quarterly Progress Report, Aug., 1957,
   p. 17; Contract No. DA-36-039 SC-73038, Armour Research Foundation,
   Chicago, Illinois.

ARMOUR RESEARCH FOUNDATION OF ILLINOIS INSTITUTE OF TECHNOLOGY

$$V_n^2 = 1/2 \left[2A^2D^2 \frac{f_{bp}}{f_r} F (1 - F) \right] = A^2D^2 \frac{f_{bp}}{f_r} F (1 - F) \tag{2}$$

The r-f "signal" in the Doppler loop in the absence of missing pulses is the magnitude of the r-f carrier, or

$$V_s = D A \tag{3}$$

This is reduced by the missing pulses to the value[2]

$$V_s = D A (1 - F) \tag{4}$$

Combining (2) and (4) gives the signal-to-noise ratio due to missing pulses alone:

$$\left(\frac{V_s}{V_n} \right)^2 = \frac{f_r}{f_{bp}} \frac{1 - F}{F} \tag{5}$$

The Doppler loop S/N ratio due to receiver noise alone has the form

$$\left(\frac{V_s}{V_n} \right)^2 = \frac{f_r}{f_{bp}} \left(\frac{V_s}{V_n} \right)_{i-f}^2 - \tag{6}$$

where $\dfrac{V_s}{V_n}$ is the S/N ratio in the radar i-f.

Comparing (5) and (6) it may be concluded that the factor $(1 - F)/F$ must be on the order of or greater than $(V_s/V_n)_{i-f}^2$ if the coherent radar performance is not to be appreciably degraded by missing pulses, or

$$\frac{1 - F}{F} = (V_s/V_n)_{i-f}^2 \quad \text{(or more)} \tag{7}$$

For a 10 db i-f S/N ratio, $F \leq 0.09$; for a 20 db i-f S/N ratio, $F \leq 0.01$

A good approximation for the fraction of missing pulses, F, and its complement, the probability of successful reply, W = 1 - F, is[3]

$$W = \frac{1}{1 + (n - W) (\mathcal{T}/T)} \qquad (8)$$

or

$$1 - F = \frac{1}{1 + \left[n - (1 - F) \ (\mathcal{T}/T)\right]} \qquad (9)$$

where $T = 1/f_r$ and $\mathcal{T}$ = beacon recovery time. From (7) and (9) we may eliminate F and obtain equivalent i-f S/N ratio, $(V_s/V_n)_{eq}$, as a function of normalized beacon recovery time, $\mathcal{T}/T$, as plotted in Fig. J-1.

For the assumed five interrogating radars (n = 5), and the resultant total interrogation rate of 5000 pps (or a PRF of 1000 pps and a period of 1000 μs per radar), Fig J-1 gives the following results.

Equivalent IF S/N Ratio $(S/N)_{eq}$	Normalized Recovery Time $\mathcal{T}/T$	Recovery Time, $\mathcal{T}$ $- \mu$s
10db	0.025	25.0
15db	0.0078	7.8
20db	0.0025	2.5

The above table indicates that recovery time shoud be kept to an absolute minimum. 25 μs recovery would appear to be the maximum allowable recovery time consistant with a useable S/N ratio.

---

[3] "Radar Systems Engineering," Rad. Lab. Series, McGraw-Hill Book Co., 1947; p. 266.
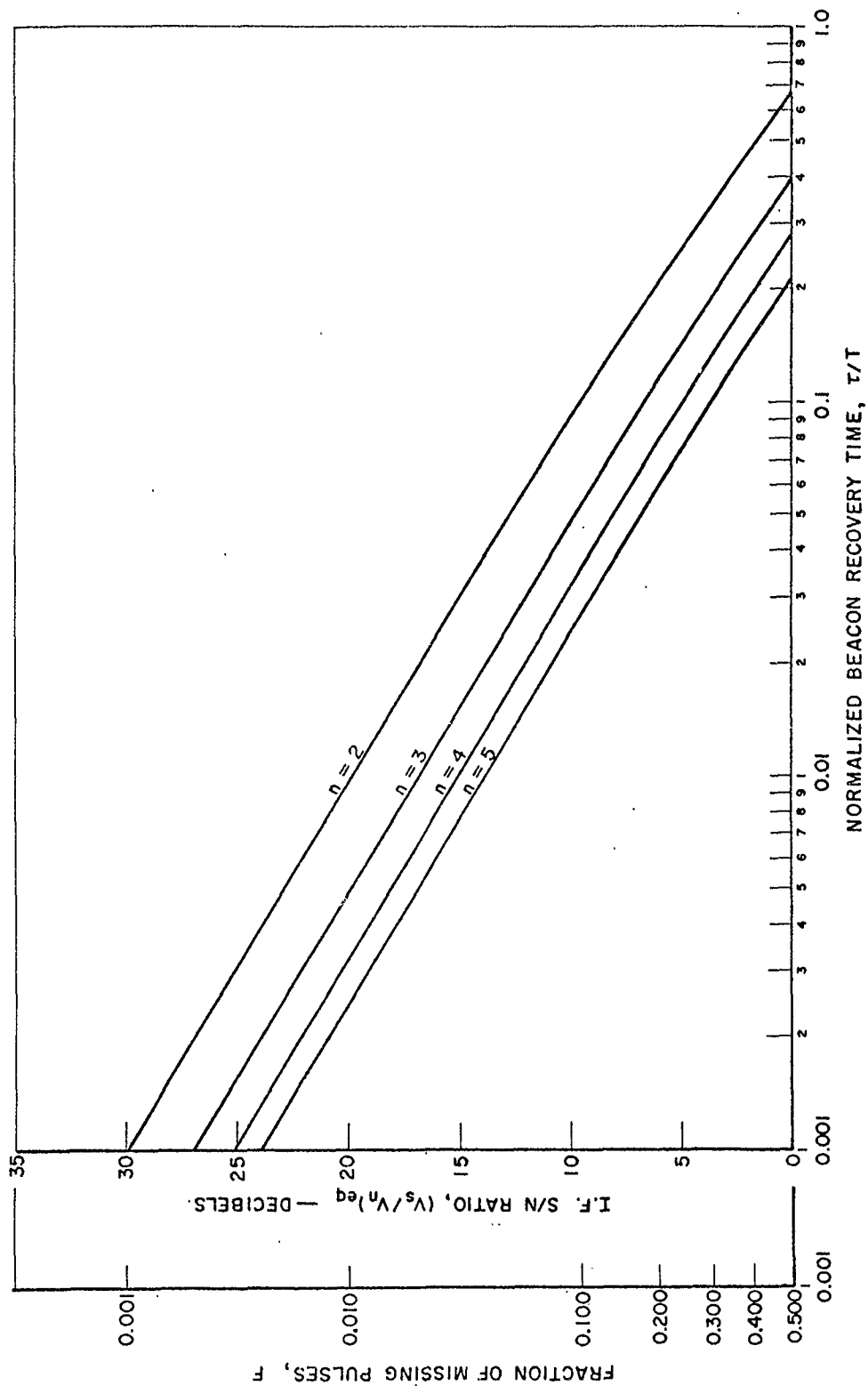
FIG J-1: EFFECT OF BEACON RECOVERY TIME ON EFFECTIVE S/N RATIO

AD _____ Div 6/6 Accession No. _____   Unclassified

Armour Research Foundation, Chicago, Illinois
EVALUATION AND IMPROVEMENT OF
RADAR BEACON SYSTEMS
R. D. Standley, S. Kazel, P. P. Toulios, J. Feldman
Third Quarterly Report
1 December 1962 - 28 February 1963
pp. 49   , illus., appendix
Contract No. DA 36-039 SC-90693

1. Radar Beacons
I. Standley, R. C.
II. Kazel, S.
III. P. P. Toulios
IV. Feldman, J.
V. U. S. A. Electronics
  Research and Develop-
  ment Laboratory
VI. Contract No. DA 36-039
  SC-90693

Unclassified Report

Theory and experimental results of a varactor tuned C-Band Tunnel Diode Oscillator are presented. Work on C-Band amplifiers is discussed with experimental results.

The dc biasing circuit of a c-band tunnel diode amplifier is analyzed and experimental results are obtained. The effect of instability in the biasing circuit is also discussed.

The fundamental limitations on the range and accuracy of coherent pulsed radar-beacon systems are analyzed. Specifications and design objectives for a coherent beacon are presented.

AD _____ Div 6/6 Accession No. _____   Unclassified

Armour Research Foundation, Chicago, Illinois
EVALUATION AND IMPROVEMENT OF
RADAR BEACON SYSTEMS
R. D. Standley, S. Kazel, P. P. Toulios, J. Feldman
Third Quarterly Report
1 December 1962 - 28 February 1963
pp. 49   , illus., appendix
Contract No. DA 36-039 SC-90693

1. Radar Beacons
I. Standley, R. C.
II. Kazel, S.
III. P. P. Toulios
IV. Feldman, J.
V. U. S. A. Electronics
  Research and Develop-
  ment Laboratory
VI. Contract No. DA 36-039
  SC-90693

Unclassified Report

Theory and experimental results of a varactor tuned C-Band Tunnel Diode Oscillator are presented. Work on C-Band amplifiers is discussed with experimental results.

The dc biasing circuit of a c-band tunnel diode amplifier is analyzed and experimental results are obtained. The effect of instability in the biasing circuit is also discussed.

The fundamental limitations on the range and accuracy of coherent pulsed radar-beacon systems are analyzed. Specifications and design objectives for a coherent beacon are presented.

AD _____ Div 6/6 Accession No. _____   Unclassified

Armour Research Foundation, Chicago, Illinois
EVALUATION AND IMPROVEMENT OF
RADAR BEACON SYSTEMS
R. D. Standley, S. Kazel, P. P. Toulios, J. Feldman
Third Quarterly Report
1 December 1962 - 28 February 1963
pp. 49   , illus., appendix
Contract No. DA 36-039 SC-90693

1. Radar Beacons
I. Standley, R. C.
II. Kazel, S.
III. P. P. Toulios
IV. Feldman, J.
V. U. S. A. Electronics
  Research and Develop-
  ment Laboratory
VI. Contract No. DA 36-039
  SC-90693

Unclassified Report

Theory and experimental results of a varactor tuned C-Band Tunnel Diode Oscillator are presented. Work on C-Band amplifiers is discussed with experimental results.

The dc biasing circuit of a c-band tunnel diode amplifier is analyzed and experimental results are obtained. The effect of instability in the biasing circuit is also discussed.

The fundamental limitations on the range and accuracy of coherent pulsed radar-beacon systems are analyzed. Specifications and design objectives for a coherent beacon are presented.

AD _____ Div 6/6 Accession No. _____   Unclassified

Armour Research Foundation, Chicago, Illinois
EVALUATION AND IMPROVEMENT OF
RADAR BEACON SYSTEMS
R. D. Standley, S. Kazel, P. P. Toulios, J. Feldman
Third Quarterly Report
1 December 1962 - 28 February 1963
pp. 49   , illus., appendix
Contract No. DA 36-039 SC-90693

1. Radar Beacons
I. Standley, R. C.
II. Kazel, S.
III. P. P. Toulios
IV. Feldman, J.
V. U. S. A. Electronics
  Research and Develop-
  ment Laboratory
VI. Contract No. DA 36-039
  SC-90693

Unclassified Report

Theory and experimental results of a varactor tuned C-Band Tunnel Diode Oscillator are presented. Work on C-Band amplifiers is discussed with experimental results.

The dc biasing circuit of a c-band tunnel diode amplifier is analyzed and experimental results are obtained. The effect of instability in the biasing circuit is also discussed.

The fundamental limitations on the range and accuracy of coherent pulsed radar-beacon systems are analyzed. Specifications and design objectives for a coherent beacon are presented.

E179
CONTRACT NO. DA-36-039 SC-90693

DISTRIBUTION LIST

Address	Copy Number
Chief Signal Officer Department of the Army Washington 25, D. C. ATTN: SIGRD	1
Commander U. S. Army Electronics Research and Development Laboratory ATTN: SIGRA/SL-SR Fort Monmouth, New Jersey	2
Commander U. S. Army Electronics Research and Development Laboratory ATTN; SIGRA /SL-SRI (Mr. Marzano) Fort Monmouth, New Jersey	3, 4
Commander U. S. Army Electronics Research and Development Laboratory ATT: SIGRA/SL-ADT Fort Monmouth, New Jersey	5
Commanding Officer U. S. Army Electronics Research and Development Activity White Sands Missile Range, New Mexico	6 thru 9
Armed Services Technical Information Agency ATTN: TIPCR Arlington Hall Station Arlington 12, Virginia	10 thru 14
Commander U. S. Naval Air Missile Test Center Point Nugu, California	15
Commander Patrick Air Force Base, Florida	16

Commander   17
U. S. Naval Ordnance Test Station
Inyokern, China Lake, California

Commander   18
U. S. Army Electronics Research and Development
    Laboratory
ATTN: SIGRA/SL-LNW (Mr. Morton).
Fort Monmouth, New Jersey

Commanding General   19
U. S. Army Ballistic Missile Agency
Huntsville, Alabama

Commander   20
Rome Air Development Center
Griffiss Air Force Base, New York

Chief   21
Bureau of Weapons
Department of the Navy
Washington 25, D. C.

Commander   22
Aeronautical Systems Division
AFSC
Wright-Patterson Air Force Base, Ohio

Commanding General   23
U. S. Army Electronic Proving Ground
Fort Huachuca, Arizona

Director   24
U. S. Naval Research Laboratory
Washington 25, D. C.

Commander   25
Air Force Cambridge Research Center
L. G. Hanscom Field
Bedford, Massachusetts

Chief   26
Bureau of Ships
Department of the Navy
Washington 25, D. C.

NOTE: All remaining undistributed copies of reports on this contract shall be forwarded to:

Airborne Instrumentation Branch
Electronic Instrumentation Division
Research and Development Department
U. S. Signal Missile Support Agency
White Sands Missile Range, New Mexico